國 立 交 通 大 學

電信工程學系

碩 士 論 文

Ku 頻段反射式類比移相器
與縮小化寬頻阻抗轉換微波岔路環

Ku Band Reflection-Type Analog Phase Shifter and Reduced-size Broadband Impedance-Transforming 180^o Hybrid Ring Coupler

研究生：陳威綸

指導教授：張志揚　博士

中華民國　九十七　年　六　月

Ku 頻段反射式類比移相器
與縮小化寬頻阻抗轉換微波岔路環

Ku Band Reflection-Type Analog Phase Shifter and Reduced-size Broadband Impedance-Transforming 180^{o} Hybrid Ring Coupler

研 究 生：陳威綸　　Student：Wei-Lun Chen

指導教授：張志揚 博士　　Advisor：Dr. Chi-Yang Chang

國立交通大學
電信工程學系
碩士論文

A Thesis
Submitted to Department of Communication Engineering
College of Electrical and Computer Engineering
National Chiao Tung University
In Partial Fulfillment of the Requirements
for the Degree of
Master of Science
In
Communication Engineering
June 2008
Hsinchu, Taiwan, Republic of China

中華民國 九十七 年 六 月

Ku 頻段反射式類比移相器
與縮小化寬頻阻抗轉換微波岔路環

研究生：陳威綸　　　　　　　　　指導教授：張志揚 博士

國立交通大學電信工程學系

摘要

本論文前半部提出兩種適用於 Ku 頻帶的類比反射式移相器：一種是將可變電容二極體諧振並轉換阻抗使可移轉角度增加到 280 度，另一種是透過並聯兩個可變電容二極體的方式使可移轉角度超過 360 度。並且，本文利用此移相器設計了一個可調整天線主波束方向的相位陣列。

本論文後半部份設計一個中心頻率為 3GHz 的寬頻微波岔路環。在各輸出入埠加上額外的單位元件(unit element 即為一段四分之一波長傳輸線)，可使頻寬接近 100%並具有阻抗轉換功能(40 歐姆到 120 歐姆)。結構上，利用步階阻抗共平面帶線可以得到理想的反相器、壓制高頻諧波、和使體積縮小為原來的 70%等優點。

Ku Band Reflection-Type Analog Phase Shifter and Reduced-size Broadband Impedance-Transforming 180° Hybrid Ring Coupler

Student: Wei-Lun Chen Advisor: Dr. Chi-Yang Chang

Department of Communication Engineering
National Chiao-Tung University

Abstract

In the first part, we propose two Ku band reflection-type phase shifters using four and two varactors to exhibit maximum phase shift of 360° and 286°, respectively. For a single varactor, the maximum phase shift is increased by resonating the varactor and impedance transforming at the input of the reflection load. The 360° phase shift results from the parallel connection of two series tuned varactors. A 4-element phased array is designed and fabricated to verify the phase shifter.

In the second part, the 180° hybrid ring adding a unit element at each port has been designed to exhibit Chebyshev response and impedance transformation. We use hybrid CPS/interdigital CPS as stepped-impedance and ideal phase inverter for size reduction of 70% and wideband performance. The fabricated 180° hybrid ring exhibits a wide bandwidth of almost 100%, and its amplitude and phase balance are less than 0.55dB and 4°, respectively. For system impedance transformation of 40Ω and 120Ω, each port of the proposed 180° hybrid ring is well-matched.

Acknowledgement

誌 謝

經過兩年的研究所生涯，終於完成了這本碩士論文。本篇論文與研究所課業得以完成，最要感謝的就是我的指導教授張志揚博士。兩年來，老師的細心教誨幫助我克服了許多研究上的難題。除此之外，老師在我的人生啟蒙上也給予了許多指導，在此由衷的感謝老師。同時感謝口試委員鍾世忠教授、邱煥凱教授與陳正中博士提供的寶貴意見，使本論文更加完善。

感謝實驗室博士班學長慧諄、金雄、鈞翔、哲慶、建育與正憲的指導，尤其是哲慶學長毫不保留的將經驗與知識傳授給我，對我的論文研究有非常大幫助，並且也感謝其他實驗室學長的幫忙。感謝實驗室同窗逸銘、智皓、人錞、獻文與逸亭在學業與生活上的陪伴與照顧，讓我能在充滿歡樂氣氛的實驗室下進行研究與學習。另外，也感謝求學過程中一路陪伴我的好友們，謝謝你們的支持與鼓勵。

最後要感謝一直支持我的家人們：爸爸、媽媽和姊姊。有你們的支持，讓我的求學過程十分順利，使我無後顧之憂的完成碩士學位。

Table of Contents

List of Tables

List of Figures

Chapter 1
Introduction

1.1 Ku band Reflection-Type Phase Shifter

The Ku band (K-under band), of which the range of frequency is 11.7-12.7 GHz for downlink and 14-14.5 GHz for uplink, is primarily used for satellite communications, especially for editing and broadcasting satellite television. The 12.2 to 12.7 GHz segment is allocated to the broadcasting satellite service (BSS). Typically, satellite television systems transmit and receive signals by antenna systems with high directivity, such as satellite dish antennas. Besides the high directivity, if a receiver of the satellite television is employed on a vehicle, an antenna system requires adaptive beamforming in order to tracking the satellite when the vehicle moving uphill and downhill. The phased array is therefore useful for beamforming in the mobile satellite television system.

Phase shifters are necessary components in a phased-array antenna system. Design of phase shifters requires consideration of many factors such as large phase shift, low insertion loss, low phase error, bandwidth, low insertion-loss variation, simple control, low dc power consumption, and low cost for commercial wireless communication. In this study, we propose two configurations of Ku band reflection-type phase shifters, in which four and two varactors are used, respectively.

In chapter two, a Ku band reflection-type analog phase shifter with 360^o phase shift is proposed. The basic circuit of the phase shifter comprises a 3-dB 90^o hybrid coupler terminated with two identical reflection loads. In order to achieve 360^o phase shift range, the reflection load is made of the parallel connection of two series tuned varactors so that there are four varactors in a phase shifter. The proposed phase shifter is designed with excellent match and linear voltage-phase relationship

In chapter three, we propose a Ku band phased array with beam steering by changing the phase between antenna elements using reflection-type analog phase shifter. Instead of using four varactors in the phase shifter proposed in chapter two, we use two varactors in this phase shifter at the cost of less phase shift. The reflection load can't achieve a phase shift of 360^o by a single varactor. This work extends the maximum phase shift, which was originally limited by the capacitance tuning range of the varactor, from 52^o to 286^o by resonating the varactor with via inductance and using $\lambda/4$ impedance transformers between the branch line coupler and the varactor. Finally, the proposed phase shifters are integrated to a 4-element phased array for beam steering. Design procedure and measurement results will be showed.

1.2 Reduced-Size Impedance-Transforming Broadband 180° Hybrid Ring

The 180° hybrid ring coupler, which is also known as the rat-race ring, is an essential component in microwave circuits, such as balanced mixers, multipliers, push-pull amplifiers and antenna feed network, etc. In chapter four, a reduced-sized impedance-transforming broadband 180° hybrid ring coupler is proposed. With a unit element at each port and an ideal phase inverter, the broadband 180° hybrid ring with impedance transformation between the input and output ports is proposed. After formulating the scattering matrix of the 180° hybrid ring, the values of circuit parameters are derived by the optimization method to fit the 180° hybrid ring to a Chebyshev response. We replace each line section by three sections of stepped impedance transmission lines using CPS/interdigital CPS structure to realize an ideal 180° phase inverter and to reduce the length of each line section. The circuit analysis, design procedure, simulation and measurement results will be discussed.

Chapter 2
360^o Reflection-Type Phase Shifter

2.1 Introduction

Reflection-type phase shifters have many advantages such as good matching, low insertion loss, simple control, and low DC power consumption, so it is popular in phase shifter design. Using active components such as varactor diodes as reflection loads was first introduced in [1]. Varactors are commonly used as reflection loads so that the phase shift is limited to the capacitance tuning range of the varactor. The maximum phase shift can be extended by resonating the varactor with an inductance or changing the port impedance of the reflection load. But even when these methods are utilized, it is difficult to achieve a phase shift of 360^o by a single varactor.

In order to get 360^o phase shift range, several approaches have been proposed. The most popular approach is to cascade two series resonant varactors with a quarter-wavelength transmission line [2] [3], which is shown in Figure 2.1(a). For the dual varactor termination, the phase shift range of the reflection load is doubled. In [4] (Figure 2.1(b)), it is shown that using tunable short-terminated combline filters as reflection load also provide double insertion phase. Another approach is the combination of two series connected varactors separated by a quarter-wave transmission line and an impedance-transforming quadrature coupler [5] (Figure 2.1(c)). The required varactor capacitance variation is smaller if the impedance ratio of the impedance-transforming quadrature coupler is enlarged. Instead of the resonant load, a ladder-type reflection type phase shifter with six varactors and seven quarter-wave transmission shown in Figure 2.1(d) is proposed [6]. The total phase shift is the sum of the tunable phase of each varactor, so it can achieve large phase shift without inductors.

In addition to all of the above, using two different series tuned varactors in a parallel connection to achieve 360^{o} phase shift was provided by B. T. Henoch and P. Tamm [7]. The author obtained a 360^{o} phase shifter which has minimum variation of total phase shift versus frequency. In [8], the original varactor impedance was transformed by the transmission line, and linear voltage-phase relationship is obtained. In this chapter, we propose a full 360^{o} phase shifter with the reflection load using two resonating loads in a parallel configuration, so there are four varactors in total. The circuit schematic is shown in Figure 2.2. The proposed phase shifter is designed with excellent match and linear voltage-phase relationship at Ku band, where parasitic effects of all components such as resistors and varactor diodes have to be considered. Detail design procedure and measurement results will be discussed.

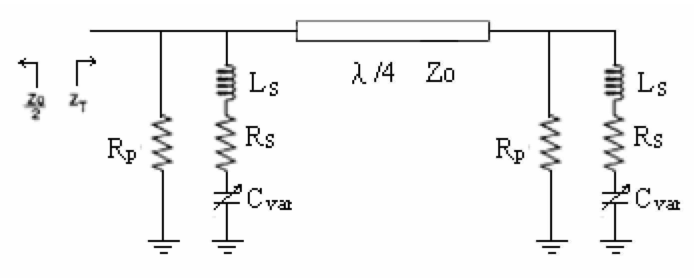

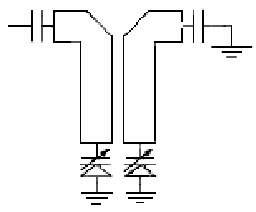

(a) (b)

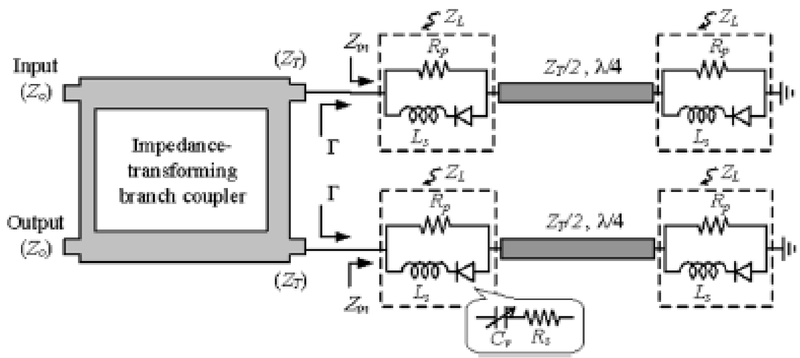

(c)

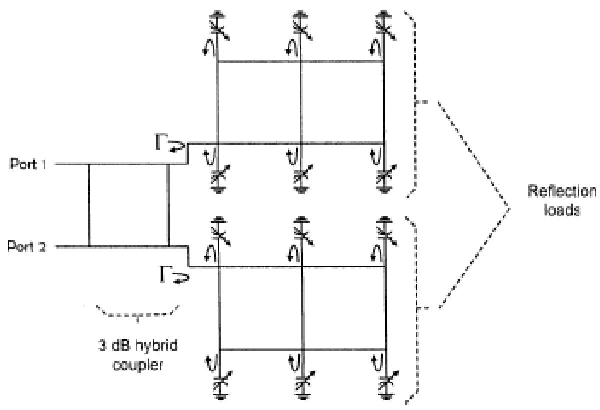

(d)

Figure 2.1: Different approaches for reflection loads of the 360° phase shifter. (a) Dual varactor termination for doubling phase shift range [3]. (b) Tunable short-terminated combline filter [4]. (c) In-series cascaded connection of varactors with the impedance-transforming quadrature coupler [5]. (d) Ladder-type reflection loads [6].

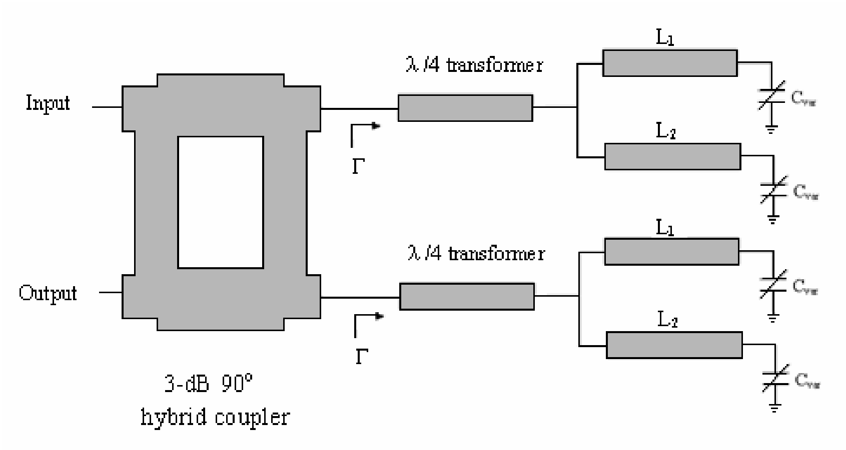

Figure 2.2: Circuit schematic of the proposed 360° reflection-type phase shifter.

2.2 Design Procedure

2.2.1 Reflection-Type Phase Shifter

As shown in Figure 2.3, a generic reflection-type phase shifter is composed of a 3-dB 90° hybrid coupler and two identical reflection loads. Due to the 3-dB hybrid 90° coupler, input signal is equally divided by the coupler in quadrature phase. The phase of reflected signal is determined by the reflection coefficient of the reflection load. Because the reflection loads are identical, two reflected signals are combined in-phase at output port. On the other hand, two reflected signals are cancelled out each other at input port. Thus, the phase shift provided by the phase shifter is equal to the phase shift of the reflection load.

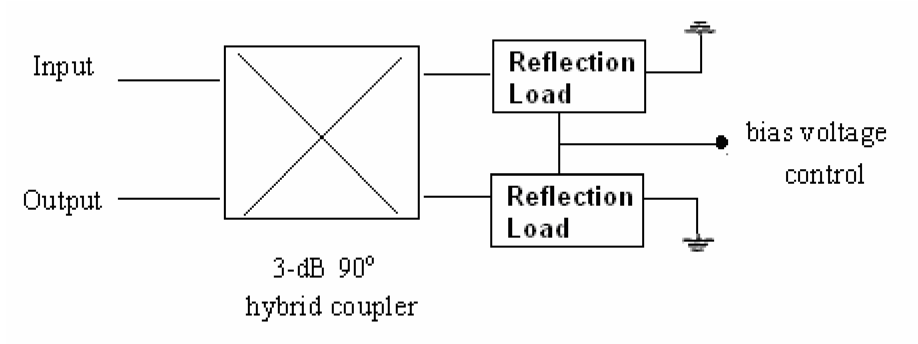

Figure 2.3: Generic reflection-type phase shifter

2.2.2 Series Resonant Varactor

The proposed phase shifter is designed at the center frequency of 12.45 GHz. MA-COM MA46H120, which is a gallium arsenide flip chip varactor diode, is used as the termination loads of the phase shifter. The circuit model is shown in Figure 2.4, where L_S, R_S, and C_P are the series inductance, series resistance, and package capacitance of the varactor diode. The tuning range of varactor capacitance C_J is from 0.2pF to 1pF. However, suffering form parasitic effects of L_S, R_S, and C_P, the characteristic of the varactor is not simply a capacitance at high frequency. Thus, the first step is to measure the characteristics of the varactor.

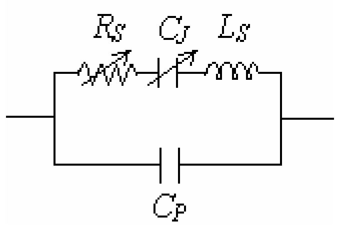

Figure 2.4: The circuit model of MA-COM MA46H120 varactor

Figure 2.5 shows two different ground structures the varactor diode mounted. The gray lines represent the microstrip line. Via holes connect the top metal to the bottom, which is a metallic ground plane. The varactor is mounted between the microstrip line and the ground area, and its reverse bias voltage is applied on the left side.

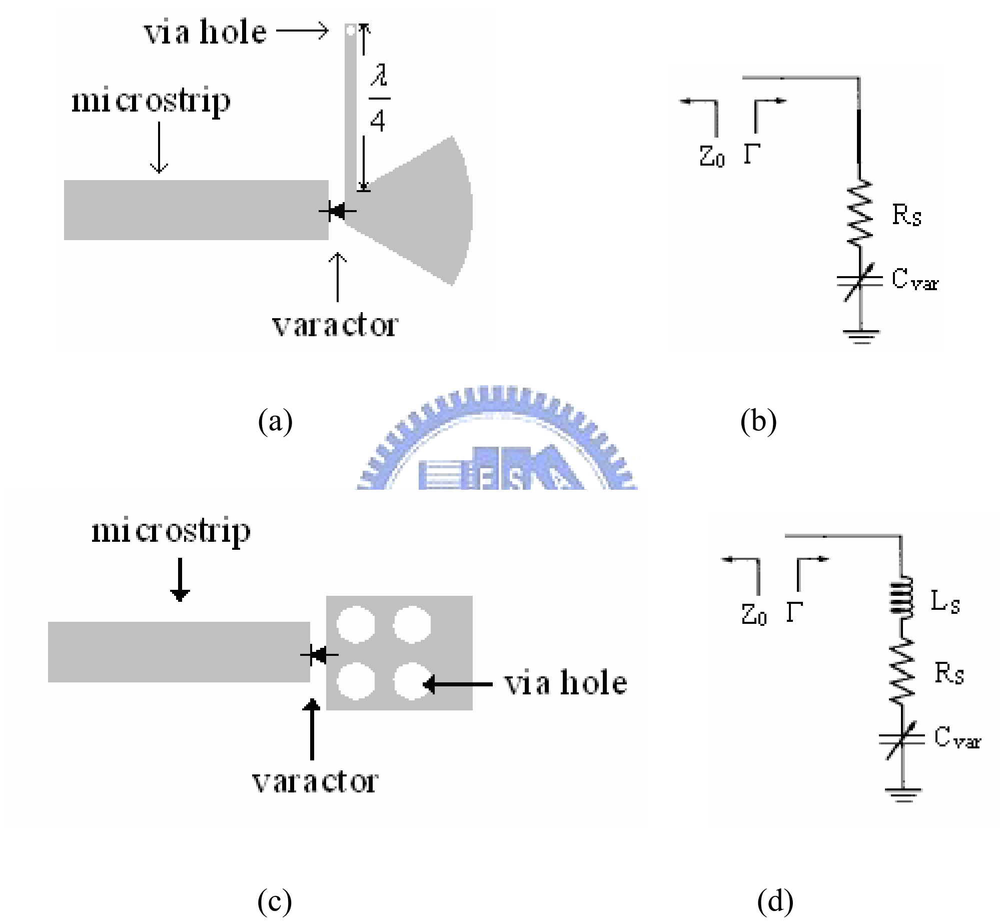

Figure 2.5: Two ground structures of termination loads.

(a) Layout of the load with RF virtual ground.

(b) Equivalent circuit of the load with RF virtual ground.

(c) Layout of series resonant loads

(d) Equivalent circuit of series resonant varactor.

Figure 2.5(a) shows that the top view of the ground structure, composed of a shunt connection of a fan stub and a quarter-wave short stub, is a RF virtual ground and DC return. A fan stub can achieve a “perfect short” over a moderate bandwidth. On the other hand, the short stub using via holes acts like a “perfect open” for RF signals, so there is no via hole effect. Thus, we can derive the characteristics of the varactor by measuring the reflection coefficient. Figure 2.5(b) shows its equivalent circuit. Measured equivalent reactance varies from -23Ω to -61Ω with tunable reactance ratio of 2.7 and total phase shift of 52^{o} at the bias voltage range of 0V to 10V. Parasitic resistance varies from 3Ω(V=0V) to 5Ω(V=10V).

In order to increase the phase shift range of the varactor, a modified ground structure is utilized, which is shown in Figure 2.5(c). The diameter of via hole is 10mil. Using ground structure in Figure 2.5(c) an inductive series reactance is added to the equivalent circuit of varactor. This via inductance can be designed to form a series resonant circuit with the varactor at the center frequency

$$\omega_0 = \frac{1}{\sqrt{L_S C_0}} \tag{2.10}$$

where L_S and C_0 represent the via inductance and the average capacitance of the varactor, respectively. With the resonance of the varactor, the impedance variation is dramatically improved and large phase shift is achieved. The circuit model is shown in Figure 2.5(d).

The characteristic of reflection loads with RF virtual ground and with via holes for ground are measured against bias voltage from 0V to 10V at 12.45GHz. Measured phase shift of reflection coefficient of varactor diodes is shown in Table 2.1. As predicted, the varactor with a RF virtual ground operates like a capacitance and has a phase shift range of 52^{o}. However, the phase shift range of the resonant varactor is improved to 119^{o}. The later is 67^{o} more than the former. The reflection coefficient of the resonant varactor is plotted for the voltage range of 0V to 10V in 1V steps on the Smith Chart in Figure 2.6, where the equivalent resistance varies with its bias voltage, as listed in Table 2.2.

Table 2.1: Measured phase of reflection coefficient of varactors at 12.45GHz

Bias Voltage(V)	$\angle\Gamma$ (degree)	
	Varactor	Resonant Varactor
0	-130	109
2	-131	128
4	-126	154
6	-103	180
8	-88	-155
10	-78	-132
Maximum phase shift	52	119

Table 2.2 Measured resistance of the resonant varactor against bias voltage.

Bias voltage(V)	0	2	4	6	8	10
Resistance(Ω)	1.4	1.7	2.1	2.6	3.2	3.8

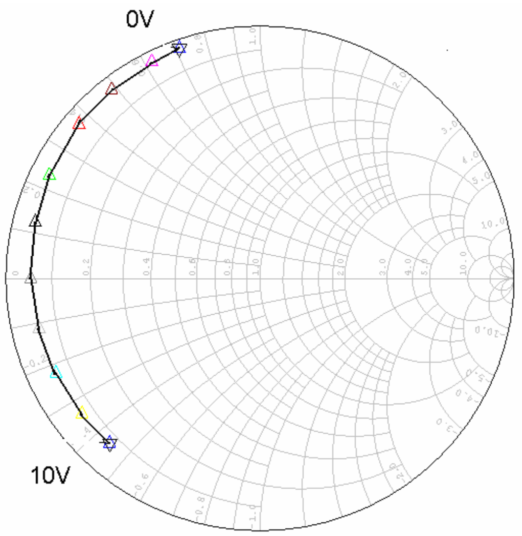

Figure 2.6: The reflection coefficient of the resonant varactor on the Smith Chart

2.2.3 Parallel Resonant Load

According to [2], if two branches of the varactors, each varactor being tuned with a series inductor to resonate at the low and high bias voltage (V_{min} and V_{max}) respectively, are connected in parallel to form a parallel resonant circuit at a control voltage between V_{min} and V_{max}, the phase shift could cover 360^{o} when the varactors are biased form V_{min} and V_{max}. This can be realized if the original resonant loads at different bias voltage are transformed by adding the transmission line with different length [9] (Figure 2.7). However, controlling the inductance of lump elements is so difficult at high frequency that transmission line is adopted in the proposed circuit.

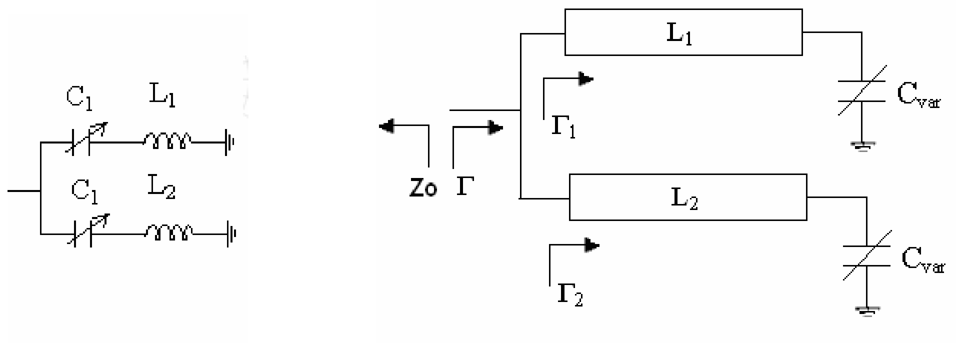

(a) (b)

Figure 2.7: Two series resonant varactor forming a parallel resonant circuit using (a) lump elements (b) transmission lines.

By tuning the length of the transmission line, the phase of each branch can be controlled arbitrarily. The reflection coefficient of each branch is shown in Figure 2.8(a), where V_0 represents the point of equal control voltage when Γ_1 and Γ_2 are complex conjugate of each other. Instead of the maximum and minimum bias voltage of 0V and 10V, the series resonance is designed at bias voltage of 2V and 9V, which will be explained later. These two branches are connected in parallel to form a 360^{o} reflective network when the varactor is biased from 2V to 9V, as shown in Figure 2.8(b). It is apparent that the reflection coefficient of the reflection load doesn't follow a constant ρ circle on the Smith Chart due to the series resistance R_S of the varactor. The resistance is 1.7Ω and 3.5Ω at the series resonance. However, at the parallel resonance the return loss is much higher because the equivalent parallel resistance is

$$R_P = (R_0 + jX_0)//(R_0 - jX_0) = \frac{R_0}{2} + \frac{X_0^2}{2R_0} \approx \frac{X_0^2}{2R_0} \qquad (2.1)$$

where R_0, X_0 represent the equivalent resistance and reactance of one branch at bias voltage of V_0. For $R_0 = 2.8\Omega$ and $X_0 = 19\Omega$, the parallel resistance R_P is approximately 65Ω and the return loss is 20dB.

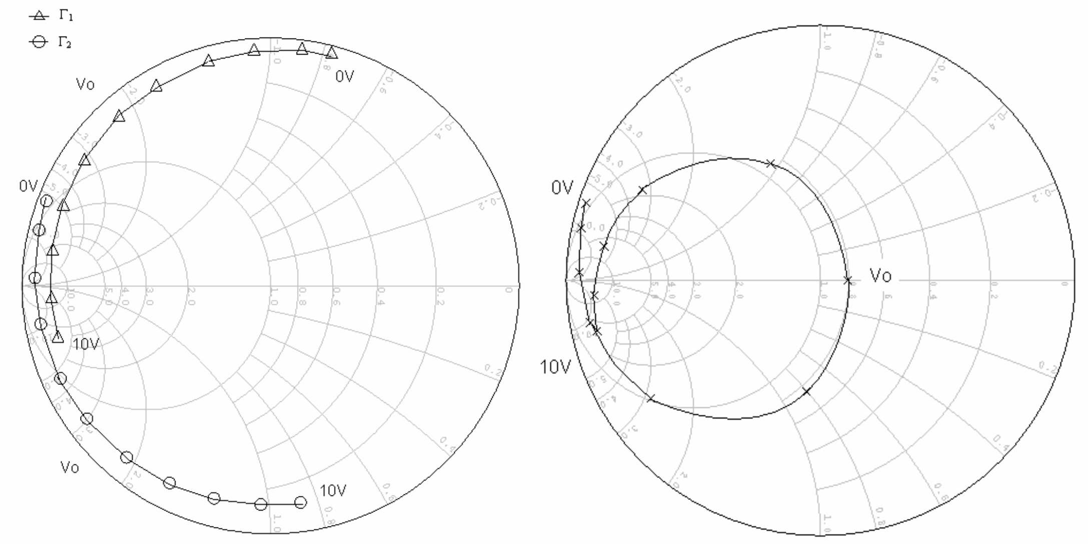

(a) (b)

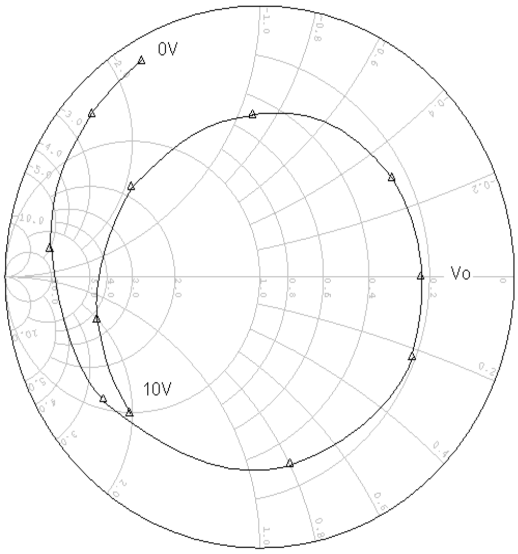

(c)

Figure 2.8: Two series resonant varactor forming a parallel resonant circuit. (a) Two series resonant varactor. (b) Parallel resonant circuit. (c) Modified parallel circuit.

2.2.4 Changing Port Impedance of Reflection Loads

In order to increase R_P and reduce the return loss at the parallel resonance, the port impedance of the reflection load is changed. For R_S and R_P giving the same reflection at series and parallel resonance, the port impedance is chosen to be

$$Z_0 = \sqrt{R_S R_P} \tag{2.2}$$

It shows that R_S is 3Ω at the series resonance point or bias voltage of 9V. Thus, from (2.2) the optimized port impedance should be 14Ω to have a minimum return-loss variation. The reason for choosing the series resonance at bias voltage of 2V and 9V is to avoid extreme R_S when bias voltage is 0, 1, and 10V. The reflection coefficient of the modified parallel circuit is shown in Figure 2.8(c).

For transforming port impedance from 50Ω to 14Ω, a quarter-wave impedance transformer is used with its characteristic impedance of 26Ω. This is too low for microstrip line to be realized. Therefore, two cascaded quarter-wave impedance transformers are used in the proposed phase shifter. The principle of impedance transforming is illustrated in Figure 2.9. The equation of the input impedance Z_{in} which is related to the characteristic impedance Z_1, is derived as

$$Z_{in} = \frac{Z_0^2}{Z_X} = \frac{Z_0^2}{\left(Z_1^2 / Z_0\right)} = \frac{Z_0^3}{Z_1^2} \tag{2.3}$$

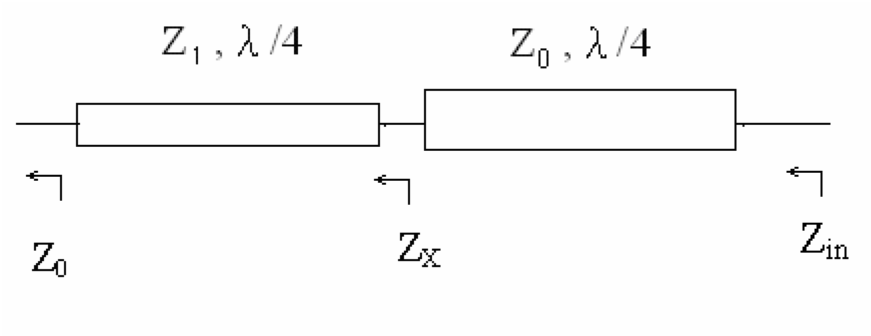

Figure 2.9: Two cascaded quarter-wave impedance transformers

If the input impedance Z_{in} is designed as 14Ω and port impedance Z_0 of 3-dB hybrid 90° coupler is 50Ω, from (2.13) the characteristic impedance Z_1 is obtained to be 90Ω. Thus, we can use two cascaded quarter-wave impedance transformers with characteristic impedance of 90Ω and 50Ω to transform port impedance from 50Ω to 14Ω over a moderate bandwidth.

2.3 Simulation Results

The proposed 360° reflection-type phase shifter is fabricated on a substrate with a dielectric constant of 3.58 and thickness of 20 mils. Full-wave EM simulation (Sonnet) is used to model the effects of via holes and tee-junctions of the branch line coupler and transmission lines. The circuit layout of the proposed circuit is shown in Figure 2.10 and the design parameters and physical dimensions are listed in Table 2.3, where W and L denote the width and length of the microstrip line, and D denotes the diameter of the via hole.

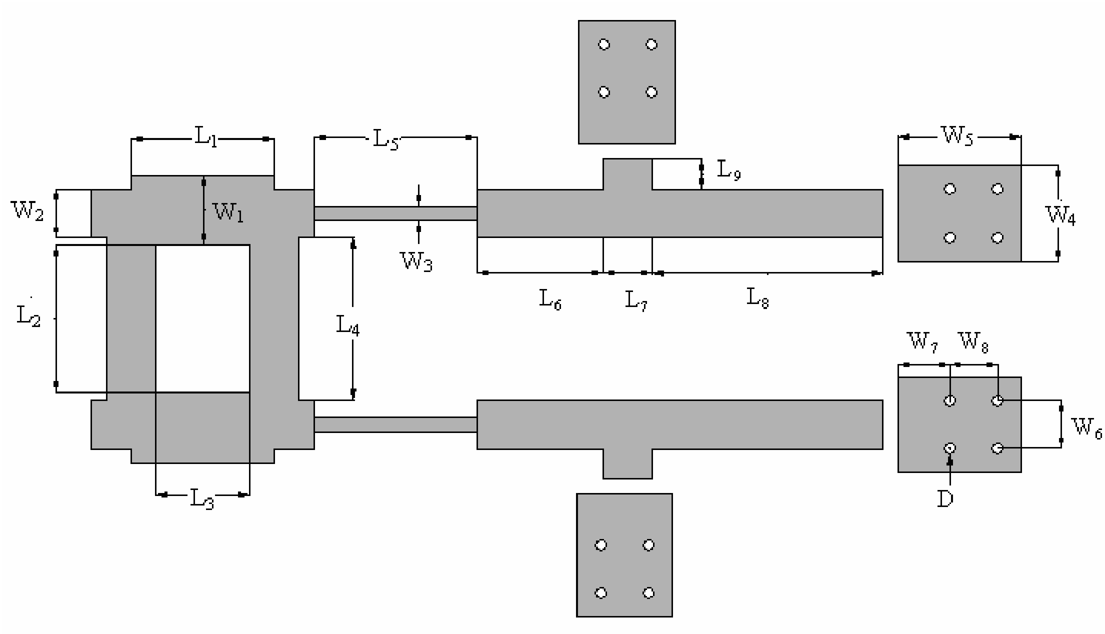

Figure 2.10: The circuit layout of the proposed 360° reflection-type phase shifter.

Table 2.3 Physical dimensions of the proposed 360° reflection-type phase shifter.

W_1	W_2	W_3	W_4	W_5	W_6	W_7	W_8	D
66	46	14	90	116	45	49	45	10
L_1	**L_2**	**L_3**	**L_4**	**L_5**	**L_6**	**L_7**	**L_8**	**L_9**
134	138	88	152	152	118	46	217	28

(Unit: mil)

The Simulated results of relative phase shift and insertion loss against control voltage at 12.45GHz are shown in Figure 2.11. With the shunt connection of two resonant loads, the phase shift of the phase shifter is more than 360° when bias voltage is raised from 0V to 10V. It shows that the insertion loss with bias voltage below 3V is much smaller than other biasing conditions. In order to minimize the fluctuation of the insertion loss, the phase shifter is designed to operate at the bias voltage of 2V-9V, and within the bias voltage a total phase shift of 360^{o} can be achieved. The scattering parameter S_{21} is plotted on the Smith Chart in Figure 2.12.

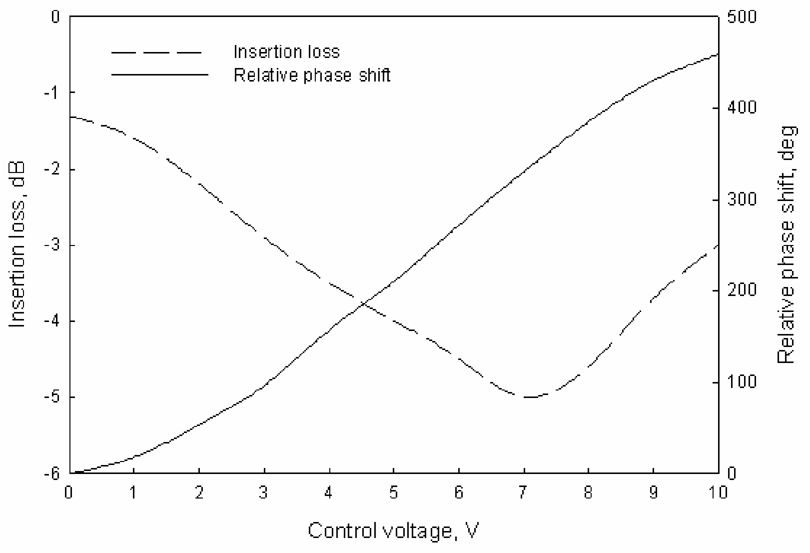

Figure 2.11: Simulated relative phase shift and insertion loss of proposed 360^{o} phase shifter at 12.45GHz.

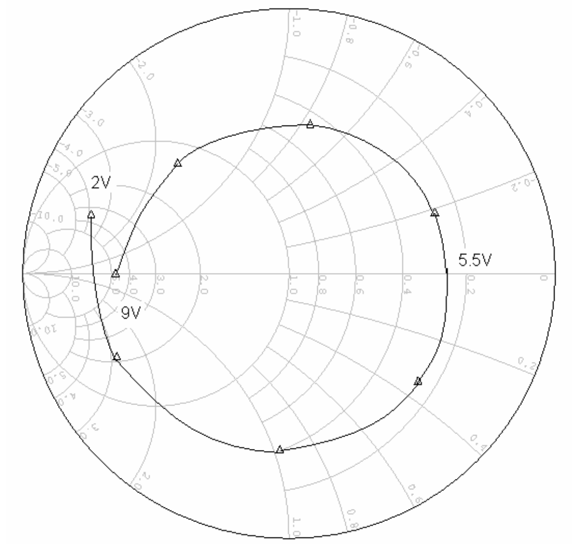

Figure 2.12: Simulated S_{21} of the proposed 360^{o} phase shifter at 12.45GHz.

2.4 Fabrication and Measurements

The 360° reflection-type phase shifter was fabricated on RO4003 substrate with a 20-mil thickness and a dielectric constant of 3.58 using a copper etching process. The diameter of via hole is 10 mils, and four flip-chip varactor diodes are mounted using a low temperature indium solder. The photograph of the proposed phase shifters is shown in Figure 2.13.

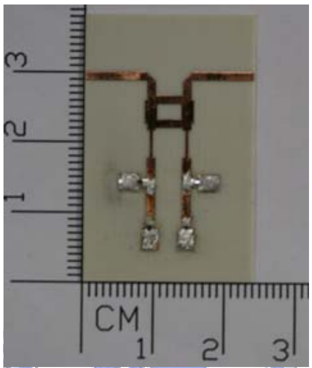

Figure 2.13: Photograph of the proposed 360° reflection-type phase shifter

2.4.1 Performance against Control Voltage

Figure 2.14 shows measured performance with respect to varactor control voltage of the proposed 360° phase shifters at 12.45 GHz. The measured maximum phase shift is 450 ° for the control voltage range of 0V-10V. It shows that for the control voltage range of 3V to 9V, a phase shift of 360° is achieved, and the average insertion loss is 5.1 dB and its variation is ± 1.3 dB. The scattering parameter S_{21}, which is plotted in Figure 2.13(c), follows nearly constant ρ circle on the Smith Chart except for the extreme control voltages. Figure 2.15 shows the comparison of relative phase shift between the proposed 360° phase shifter, series resonant varactor, and a single varactor.

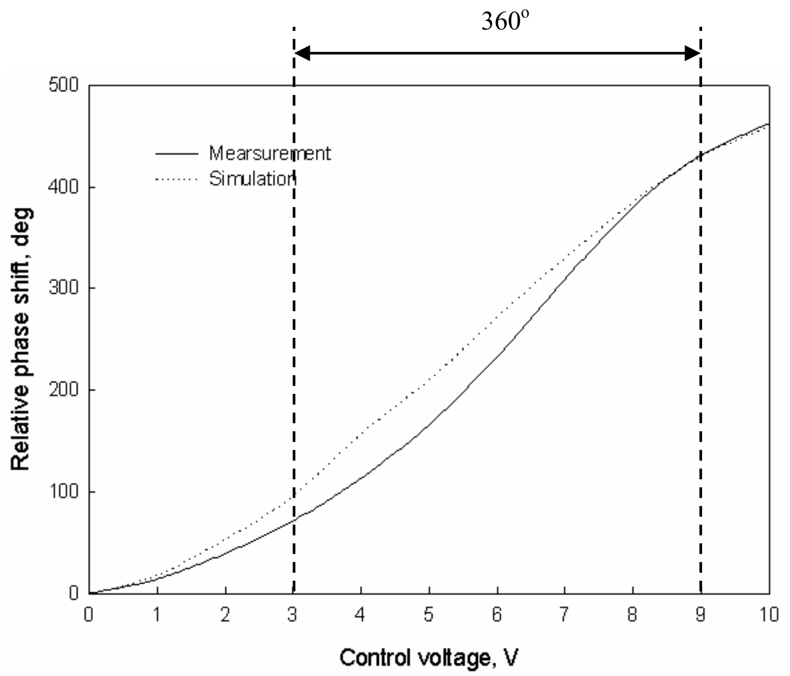

(a)

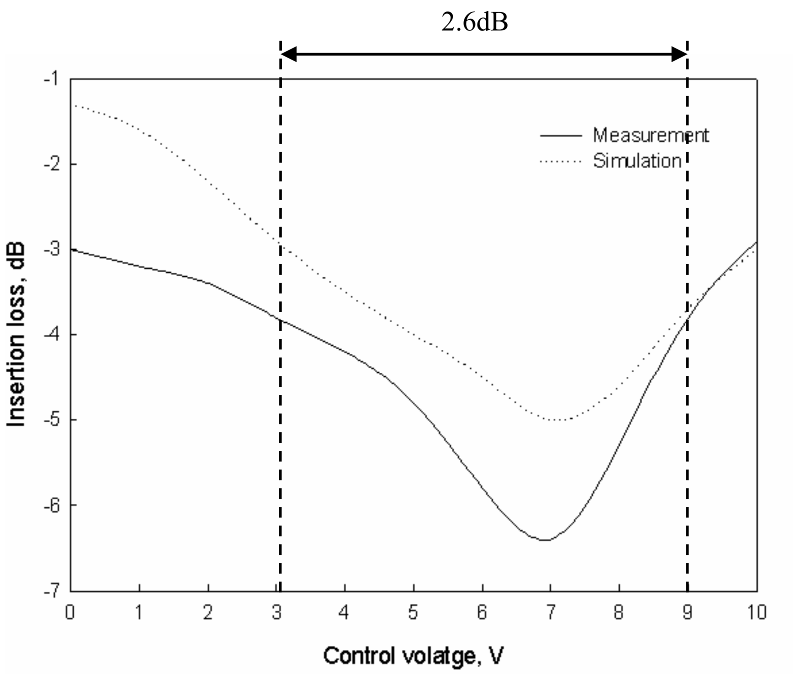

(b)

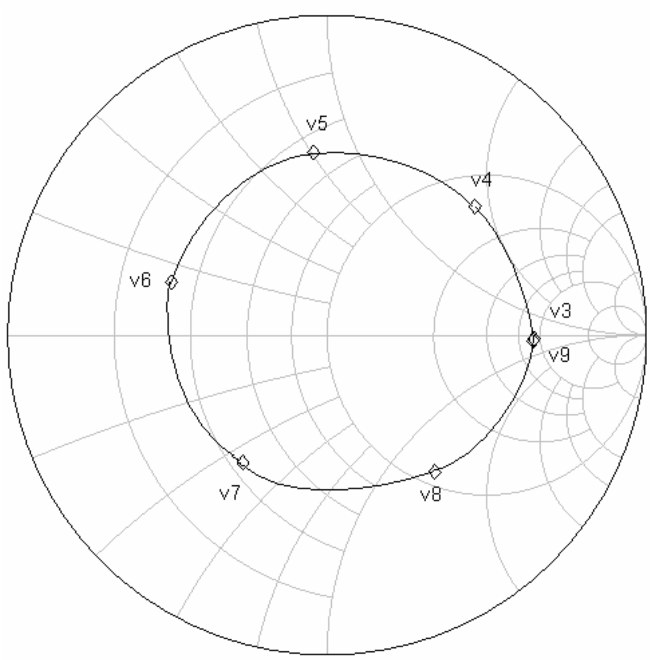

(c)

Figure 2.14: Measured results of the proposed 360° phase shifter against control voltage at 12.45GHz. (a) Relative phase shift. (b) Insertion loss. (c) S_{21} on Smith Chart.

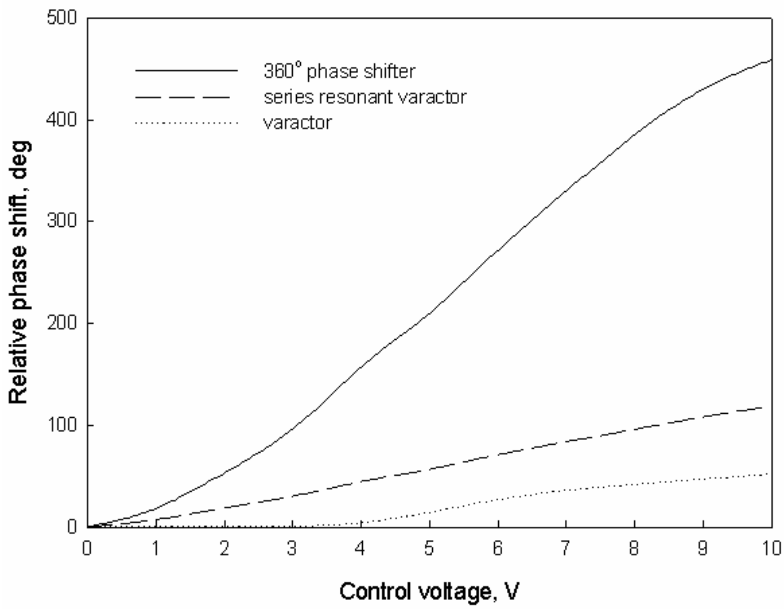

Figure 2.15: Comparison of relative phase shift between the proposed 360° phase shifter, series resonant varactor, and a single varactor.

2.4.2 Performance against Frequency

The measured frequency response is measured in Figure 2.16 from 12.2 to 12.7 GHz. The measurement is plotted at control voltage of 3V-9V, where a full 360° phase shifter is achieved. It shows that the maximum phase shift is larger than 360°, insertion loss is 4.8 ± 1.6 dB, and return loss is better than 14 dB over 500MHz of the voltage stage of 3V-9V.

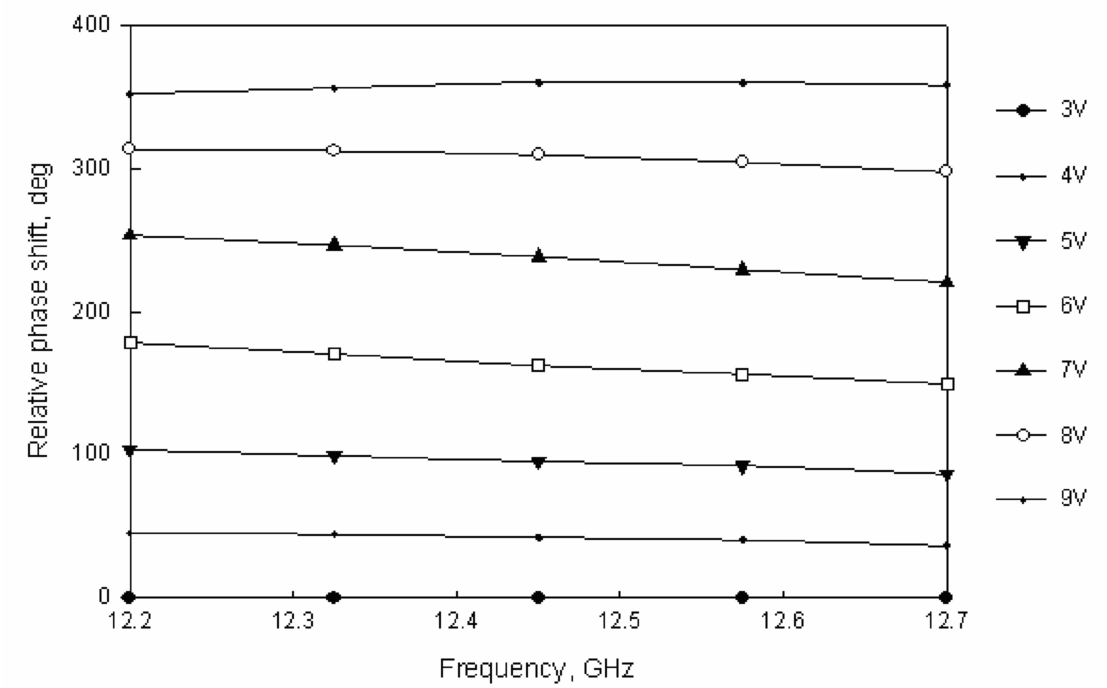

(a)

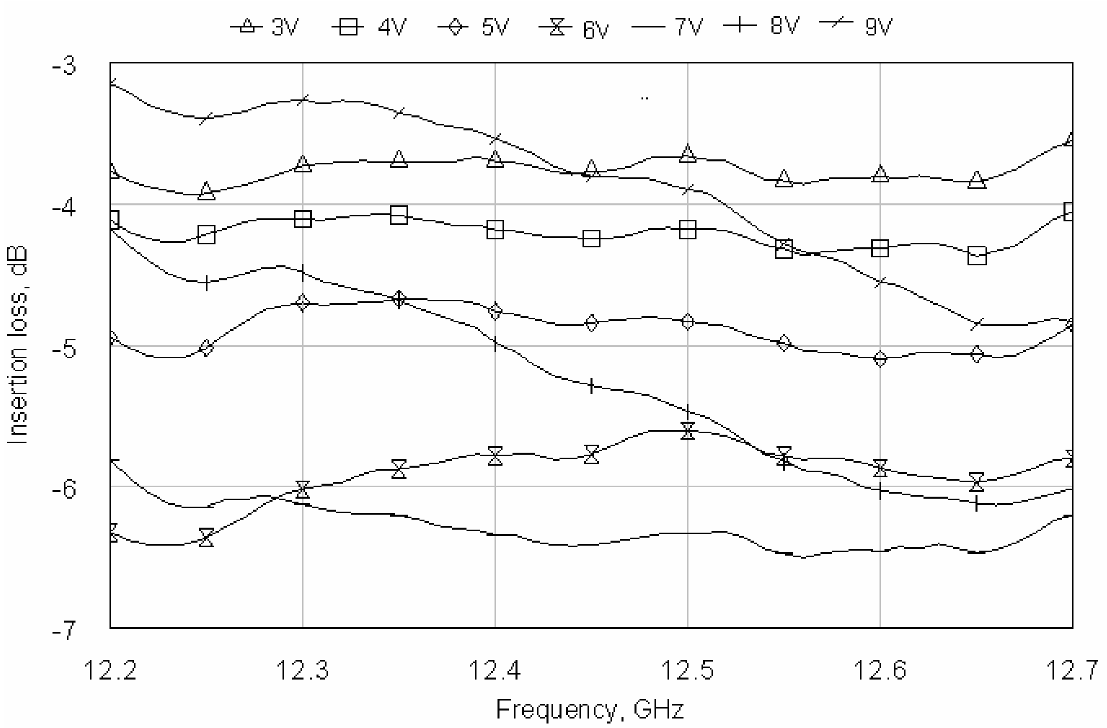

(b)

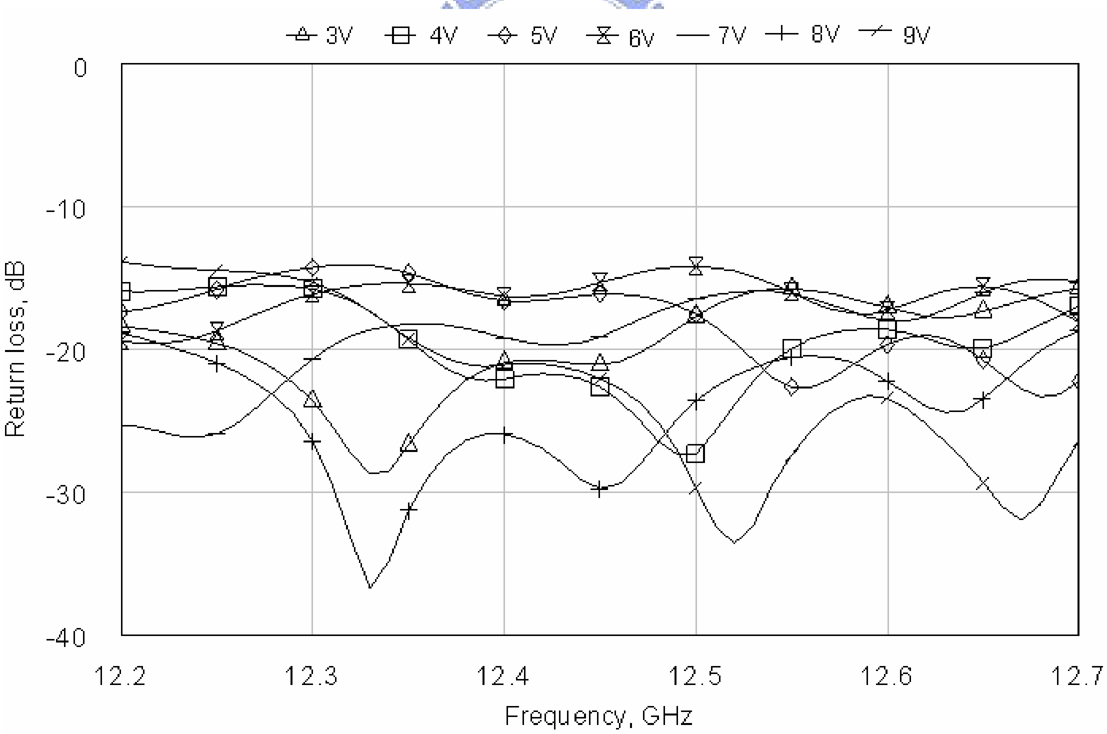

(c)

Figure 2.16: Frequency response of the 360^{o} phase shifter. (a) Relative phase shift. (b) Insertion loss. (c) Return loss.

Chapter 3
Ku band Phased array

3.1 Introduction

Phased array plays an important role in microwave applications such as radar systems and smart antenna systems of wireless mobile communication. In a phased-array antenna system, phase shifters are used to control the radiation direction. These phase shifters have to meet high requirements for continuously adjustable phase shift. Design of these phase shifters requires consideration of many factors such as large phase shift, low insertion loss, low phase error, bandwidth, low insertion-loss variation, simple control, low DC power consumption, and low cost for commercial wireless communication.

Reflection-type phase shifters (RTPS) have the advantages of simple control, low reflection, and low insertion loss. Using active components such as varactor diodes as reflection loads was first introduced in [1]. Thus, phase shift is restricted by tunable capacitance of varactor diodes. In order to maximize phase shift range of reflection loads, many approaches were reported. But when working on an effort to increase the phase shift range of phase shifters, insertion-loss variation increases. This insertion-loss variation can be eliminated by adding a compensating resistance parallel to the reflection load [2]. Furthermore, in adaptive antenna receivers, the insertion loss and the insertion-loss variation can be compensated by the variable-gain low-noise amplifiers (VGLNA) located in front of the phase shifters.

In this chapter, a Ku band (12.2-12.7GHz) phased array using reflection type analog phase shifter is proposed. First, a phase shifter with large phase shift is discussed. Instead of using two varactors for each reflection load of the proposed 360^{o} phase shifter in the previous chapter, the phase shifter uses only one varactor as the reflection load. We extends the maximum phase shift of the varactor, which was originally limited by the capacitance tuning range, from 52^{o} to 286^{o} by resonating the varactor with via inductance and using impedance transformers between the branch line coupler and the varactor. The circuit analysis, design procedure, and tradeoffs between phase shift range and insertion-loss variation are elaborately discussed. Finally, a 4-element phased array with a group of dipole antennas and the proposed phase shifters is fabricated to verify the proposed phase shifter. Low noise amplifiers (LNA) are used to compensate the insertion loss of phase shifters.

3.2 Theory of Reflection-Type Phase Shifter

The basic building block of the reflection-type phase shifter composed of a 3-dB 90^{o}

hybrid coupler and two identical reflection loads has been discussed in chapter two. In this chapter, however, the phase shifter uses only one varactor for each reflection load. The analysis, design procedure, and fabrication of the phase shifter will be discussed.

3.2.1 Analysis

In the simplest design, a single varactor used as reflection loads is shown in Figure 3.1(a). The phase of reflection coefficient is determined by the maximum capacitance variation of the varactor diode. The phase shift can be increased by adding an inductance L_S in series to the varactor, forming the series resonant circuit (Figure 3.1(b)). The maximum phase shift range is achieved at the resonance frequency

$$\omega_0 = \frac{1}{\sqrt{L_S C_0}} \tag{3.1}$$

where C_0 represents the average capacitance value of the varactor.

To simplify this model, the parasitic resistance of the varactor and series inductance is combined as R_S. Also, the inductance L_S includes the parasitic inductance of the varactor. In the ideal case ($R_S = 0$), the phase shift of reflection coefficient follows the unity circle of the Smith Chart. But for real varactor diodes with finite Q, the effective series resistance R_S must be included in the circuit model. In this case, the reflection coefficient follows a constant resistance circle on the Smith Chart, and this series resistance determines the insertion loss and insertion-loss variation with the varactor bias voltage.

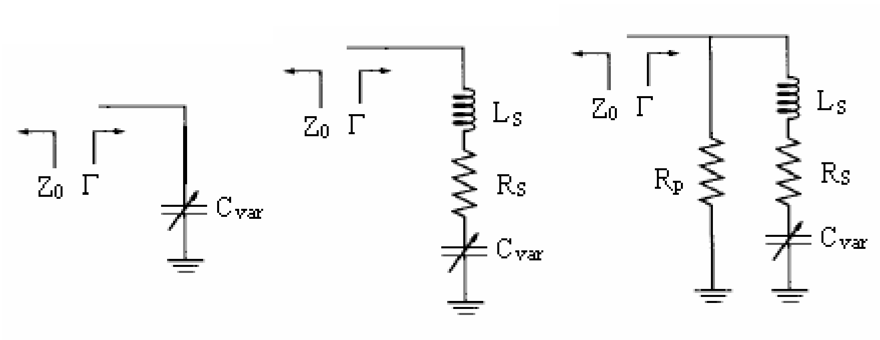

(a) (b) (c)

Figure 3.1: Circuit model of reflection loads, (a) Varactor. (b) Series resonant varactor. (c) Series resonant loads with compensating resistance.

A method for compensating the insertion-loss variation is to shunt a resistance R_P to the series resonant load as shown in Figure 3.1(c). This compensating resistance is used to transform the constant resistance circle locus to a constant ρ circle on the Smith Chart. Then, the insertion loss maintains nearly constant and insensitive with the change of varactor bias voltage.

3.2.2 Design Formula

The reflection coefficient Γ of the reflection load in Figure 3.1(c) is given by

$$\Gamma = |\Gamma| e^{j\phi} = \frac{(R_p R_s + R_p Z_0 - R_s Z_0) + jX_L(R_p - Z_0)}{(R_p R_s + R_p Z_0 + R_s Z_0) + jX_L(R_p + Z_0)} \tag{3.2}$$

where X_L is equal to $\omega L_S - 1/\omega C_{\text{var}}$. Thus, phase shift and return loss of the reflection load are

$$\phi = \tan^{-1}\frac{X_L(R_p - Z_0)}{R_pR_s + R_pZ_0 - R_sZ_0} - \tan^{-1}\frac{X_L(R_p + Z_0)}{R_pR_s + R_pZ_0 + R_sZ_0} \tag{3.3}$$

$$\text{RL} = |\Gamma|^2 = \frac{(R_pR_s + R_pZ_0 - R_sZ_0)^2 + X_L{}^2(R_p - Z_0)^2}{(R_pR_s + R_pZ_0 + R_sZ_0)^2 + X_L{}^2(R_p + Z_0)^2} \tag{3.4}$$

Since reflected signals are combined from two identical reflection loads at the output of the 3-dB 90° hybrid coupler, the scattering parameter S_{21} of the phase shifter is obtained as $j\alpha^2\Gamma$, where α is the loss of the 3-dB 90° hybrid coupler. Phase shift $\angle S_{21}$ and insertion loss $|S_{21}|$ of the phase shifter is

$$\angle S_{21} = \phi + \frac{\pi}{2} = \tan^{-1}\frac{X_L(R_p - Z_0)}{R_pR_s + R_pZ_0 - R_sZ_0} - \tan^{-1}\frac{X_L(R_p + Z_0)}{R_pR_s + R_pZ_0 + R_sZ_0} + \frac{\pi}{2} \tag{3.5}$$

$$\text{IL} = \alpha^2|\Gamma|^2 = \alpha^2\frac{(R_pR_s + R_pZ_0 - R_sZ_0)^2 + X_L{}^2(R_p - Z_0)^2}{(R_pR_s + R_pZ_0 + R_sZ_0)^2 + X_L{}^2(R_p + Z_0)^2} \tag{3.6}$$

From (3.5) and (3.6), the varactor reactance determines not only the relative phase shift but also the insertion loss. The maximum phase shift $\Delta\phi$ is

$$\Delta\phi = \angle S_{21}\Big|_{X_{L,\max}} - \angle S_{21}\Big|_{X_{L,\min}} \tag{3.7}$$

For a given varactor capacitance range, the maximum phase shift can be increased by lowering the impedance level Z_0 at the input of the reflection load, while the input and output impedance level of the 3-dB 90° hybrid coupler is unchanged.

To eliminate the insertion-loss variation, $|\Gamma|$ must be constant whatever the varactor capacitance is. Detailed equations have been derived in [9] to achieve maximum phase shift while remaining insertion loss constant. The optimal compensating resistance is derived as

$$R_{comp} = \frac{Z_0^2}{2R_s}\left[1+\sqrt{1+\left(\frac{2R_s}{Z_0}\right)^2}\right] \tag{3.8}$$

While the maximum relative phase shift with constant insertion loss is

$$\Delta\phi_{\max} = 4\tan^{-1}\left[\frac{\Delta X_L}{2Z_0}\frac{Z_0(Z_0+\sqrt{Z_0^2+4R_S^2}+2R_S)}{(Z_0+R_S)(Z_0+\sqrt{Z_0^2+4R_S^2})+2R_S^2}\right] \tag{3.9}$$

3.3 Design Procedure of Ku Band Reflection-Type Phase Shifter

The design procedure of the proposed Ku band reflection-type phase shifter is as the following steps:

Step 1) Measure the characteristics of the varactor. Then, resonate the varactor by adding a series inductance L_S.

Step 2) Change port impedance of the reflection load depending on the required maximum phase shift. Phase shift may be increased by lowering the impedance level Z_0. Optimum design uses highest Z_0 to produce necessary phase shift range

Step 3) Add a resistance parallel to the reflection load to compensate the insertion loss variation.

3.3.1 Series Resonant Varactor

The varactor diode MA-COM MA46H120 is used as the termination load of the proposed 360^{o} reflection-type phase shifter. In the previous chapter, we have shown to extend the phase shift from 52^{o} to 119^{o} with the resonant load by adding via inductance to the varactor.

3.3.2 Changing Port Impedance of Reflection Loads

For a given varactor capacitance range, the maximum phase shift can be increased by lowering the impedance level Z_0 at the input of the reflection load. Since the resonant inductance L_S of the proposed phase shifter is made of via holes, the value of L_S is somewhat different to the optimal resonant inductance. In order to achieve maximum phase shift, a short transmission line L_1 with phase delay of 6^{o} is added in front of the varactor load as shown in Figure 3.2(a). The transmission line changes the phase of reflection coefficient of the reflection load, making the maximum and minimum phase of reflection coefficient vertically symmetry on the Smith Chart, as shown in Figure 3.2(b).

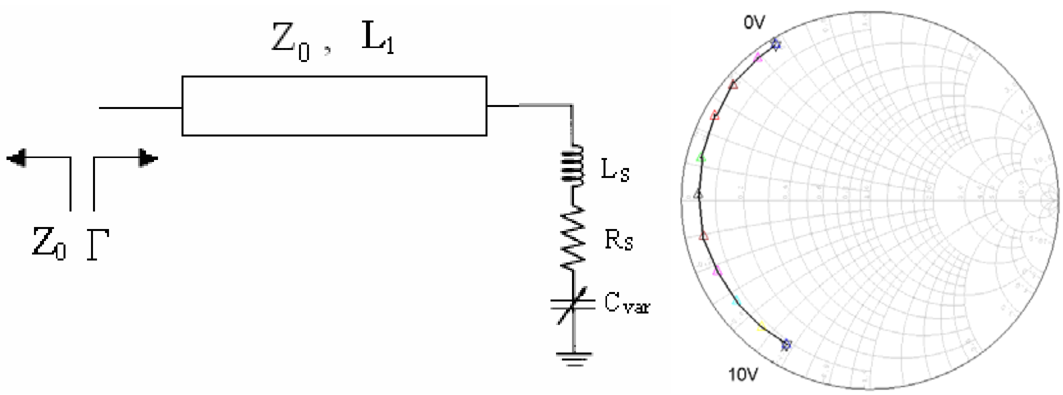

(a) (b)

Figure 3.2: (a) Varactor load with a transmission line with L_1=6°. (b) Reflection coefficient on the Smith Chart.

To simplify the effect of the port impedance on the maximum relative phase shift, the cases of reflection loads without compensating resistance R_P is considered. Figure 3.3 shows examples of reflection coefficient with different Z_0 of 25Ω and 12.5Ω on the Smith Chart. It is shown that lowering the port impedance Z_0 increases not only the maximum phase shift but also insertion-loss variation, which is the tradeoff of phase shifter design. Figure 3.4 shows design charts of maximum phase shift values and insertion-loss variations of phase shifter with respect to port impedance Z_0.

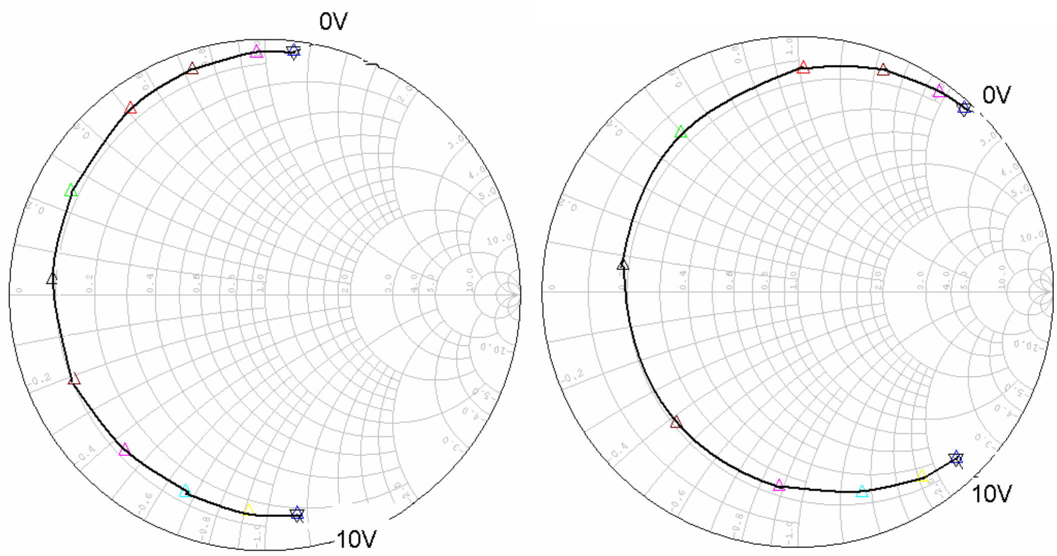

(a) (b)

Figure 3.3: Reflection coefficient of reflection loads at 12.45 GHz.

(a) Z_0=25Ω, maximum phase shift = 195°. Insertion loss variation = 1.4dB.

(b) Z_0=13Ω, maximum phase shift = 266°. Insertion loss variation = 2.8.dB.

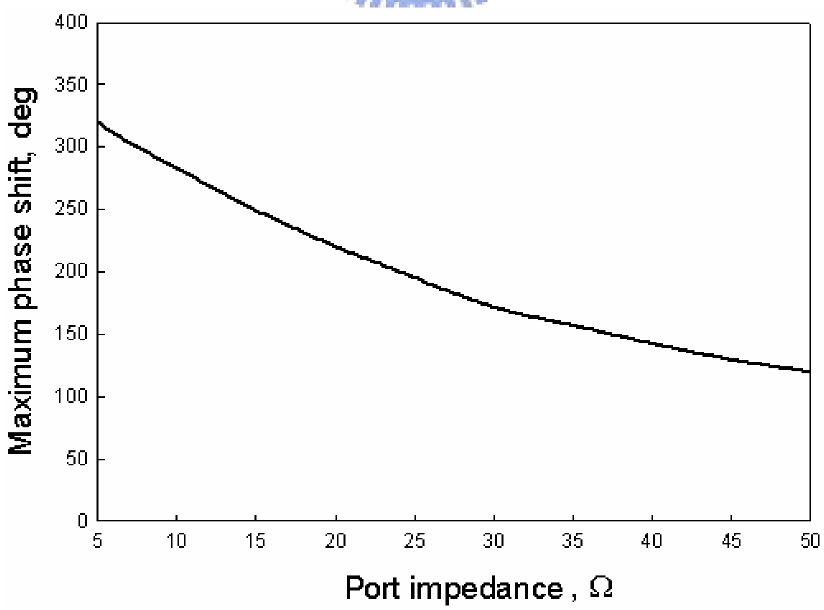

(a)

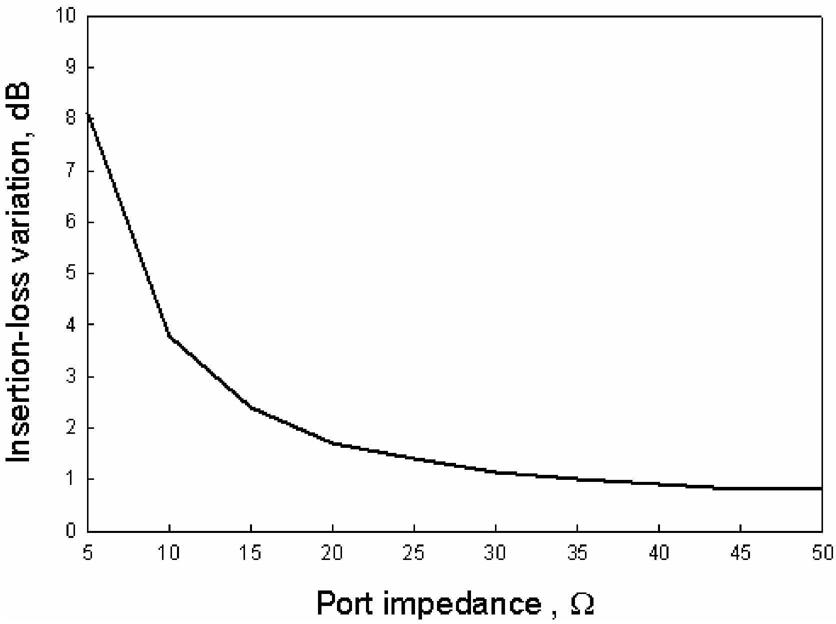

(b)

Figure 3.4: (a) Maximum phase shift and (b) Insertion loss variation against port impedance Z_0

In [9], an impedance-transforming branch line coupler is applied to the phase shifter. However, if the required impedance Z_0 is very low, the impedance transforming branch line coupler is too hard to be realized. In the proposed phase shifter, Z_0 was designed at 9Ω, which is impossible for microstrip line fabrication. So, two cascaded quarter wave impedance transformers are implemented between a conventional 3-dB 90^{o} hybrid coupler and the reflection load to produce an adequately low impedance level.

Figure 3.5 shows total reflection load with impedance transformers. Comparison of relative phase shift with and without impedance transformers is depicted in Figure 3.6. With the help of two cascaded impedance transformers, maximum phase shift of 292^o, which is 173^o more than the other one, is given with the same bias voltage condition.

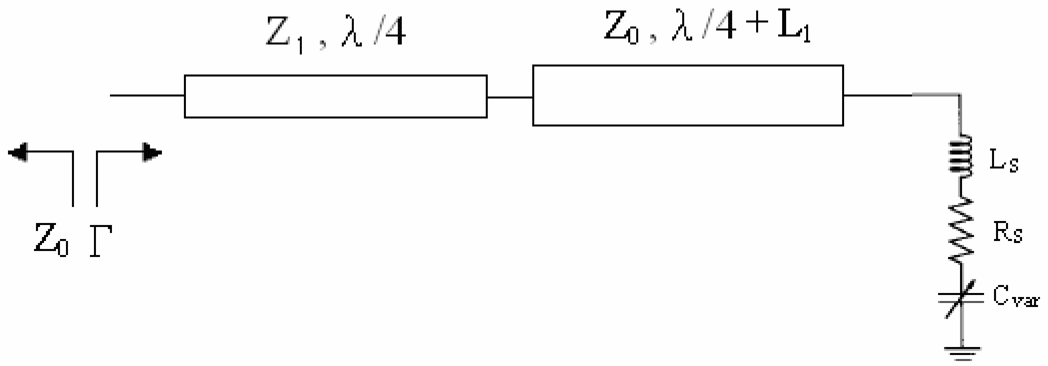

Figure 3.5: Reflection load with two cascaded impedance transformers. Z_1=118Ω, Z_0=50Ω, L_1=6^o

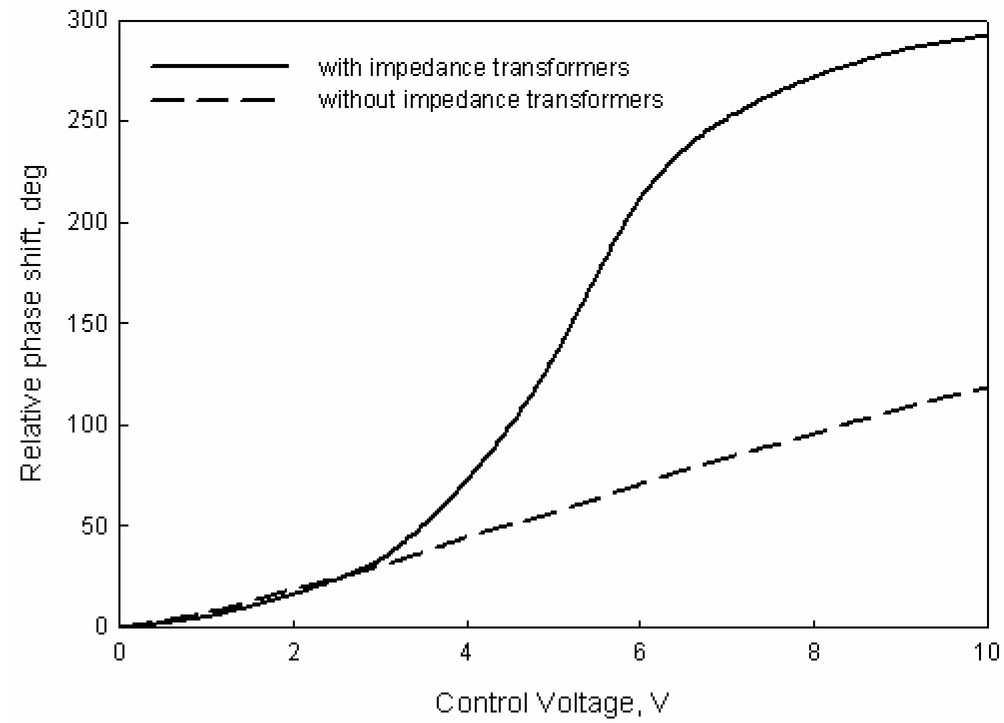

Figure 3.6: Comparison of phase shift of the reflection load with and without impedance transformers.

3.3.3 Compensation for Insertion-Loss Variation

Given in Figure 3.4, the insertion-loss variation is 4.3 dB for the phase shifter when maximum phase shift of 292^{o} is chosen. With the help of a compensation resistance R_P parallel to reflection loads shown in Figure 3.7, insertion-loss variation can be eliminated. The optimized compensating resistance R_P is chosen to be 200Ω. The principle of compensation for insertion-loss variation is illustrated in Figure 3.8. Equivalent conductance at high/low control voltage is dominated by the compensating resistance. With optimized R_P, the reflection coefficient of the reflection load follows almost constant ρ circle on the Smith Chart. However, constant insertion loss is unavailable because R_S varies with the bias voltage. But (3.8) is still useful for initial design.

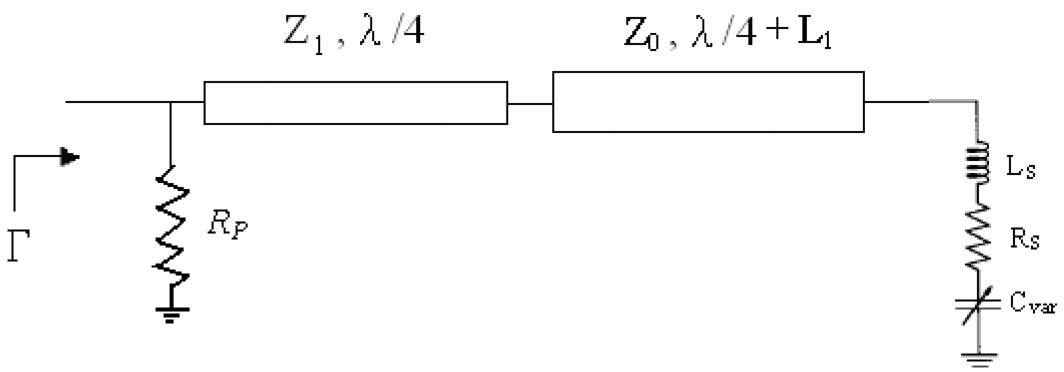

Figure 3.7: Reflection load with compensating resistance R_P. Z_1=118Ω, Z_0=50Ω, L_1=6^{o}, R =200Ω

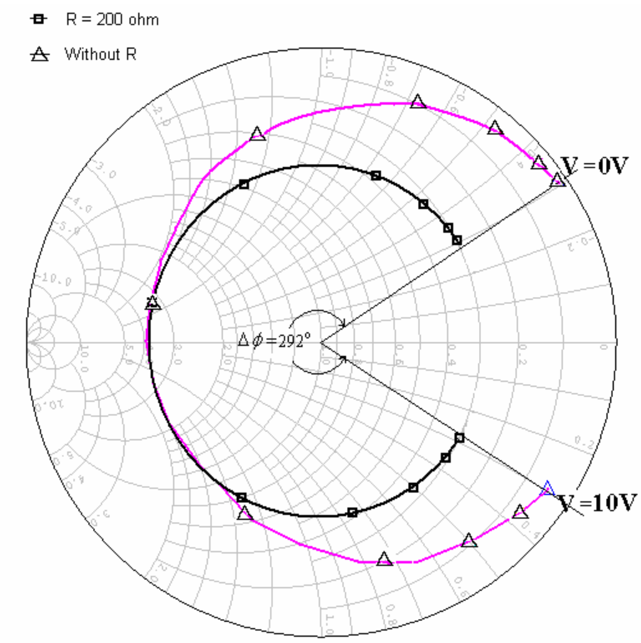

Figure 3.8: Reflection coefficient of the reflection load on the Smith Chart.

Figure 3.9 shows simulated reflection coefficient of reflection loads with and without R_P. With R_P =200Ω, insertion-loss variation is 1 dB and maximum phase shift is 287°. The use of R_P barely influences maximum phase shift range.

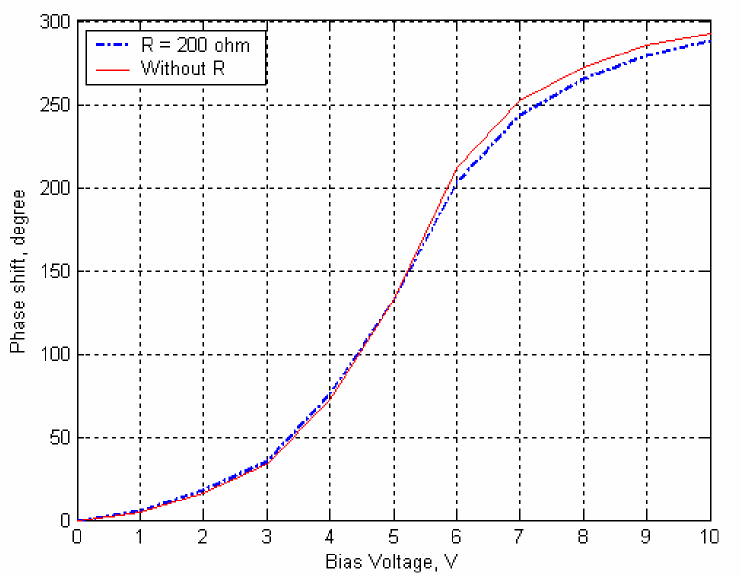

(a)

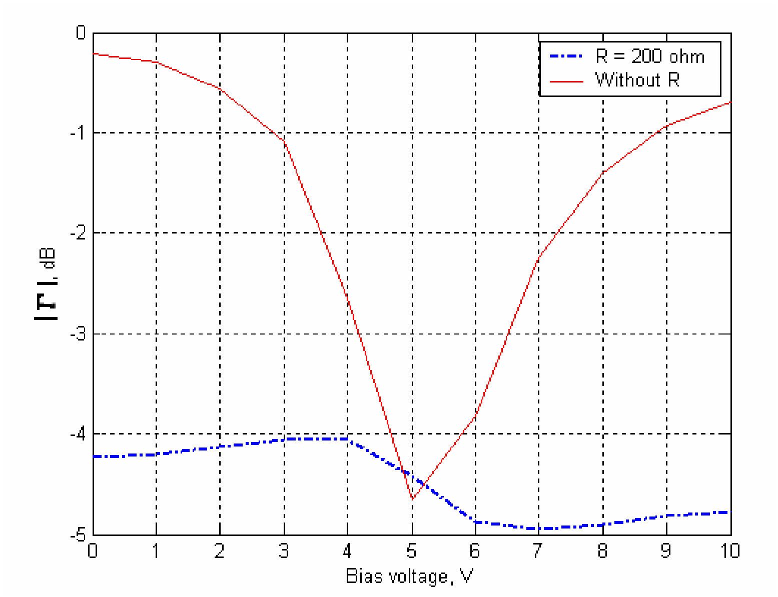

(b)

Figure 3.9: Comparison of simulated reflection loads with and without R_P at 12.45 GHz. (a) Relative phase shift and (b) Return loss of the reflection load against bias voltage of varactor.

3.4 Fabrication and Measurements of Ku Band Reflection-Type Phase Shifter

The proposed reflection-type phase shifter was fabricated on RO4003 substrate with a dielectric constant of 3.58 and thickness of 20 mils to verify the phase shifter design procedure. The phase shifters were designed with and without the compensating resistance R_P, which has been described in detail at the pervious section. Then, a 3-dB 90^o hybrid coupler with the characteristic impedance of 50Ω at the center frequency of 12.45 GHz was terminated with two identical designed reflection loads. The 0402

220Ω chip resistor with fan stub as ground was used as the compensating resistance R_P. The photograph of the proposed phase shifters is shown in Figure 3.10.

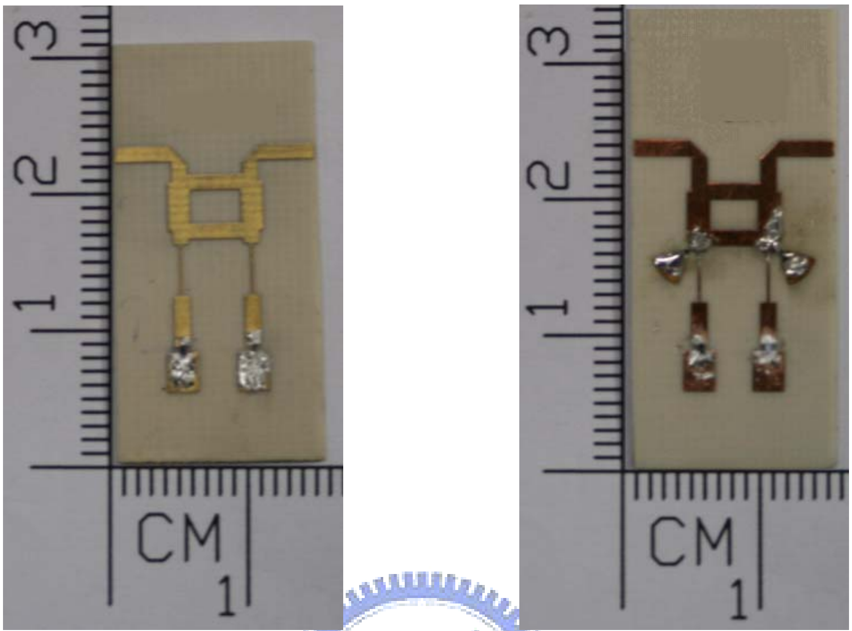

(a) (b)

Figure 3.10: Photograph of the proposed phase shifter circuits (a) without R_P (b) with R_P=220Ω

3.4.1 Performance against Control Voltage

Figure 3.11 shows measured performance with respect to varactor control voltage of the proposed two phase shifters without R_P and with R_P =220Ω. The measured maximum phase shift of phase shifter is 286° without R_P and 283° with R_P =220Ω. In Figure 3.9(a), the simulated maximum relative phase shift, which is 292° without R_P and 287° with R_P=200Ω, agrees well with the measured results.

The measured insertion-loss variation of phase shifter is 4 dB without R_P and 3.5 dB with R_P=220Ω. In Figure 3.9(b), the simulated insertion loss variation is 4.5 dB without R_P and 1 dB with R_P=200Ω. The measured insertion loss of phase shifter without R_P agrees with the simulated results. But in the case of R_P=220Ω, the compensating resistance slightly influences the insertion-loss variation. This is mainly because the unwanted package capacitance of the chip resistor is parallel to the reflection load at high frequency of 12.45 GHz. The parallel capacitance and other parasitic effect can be observed from the S_{21} of the phase shifter on the Smith Chart shown in Figure 3.12.

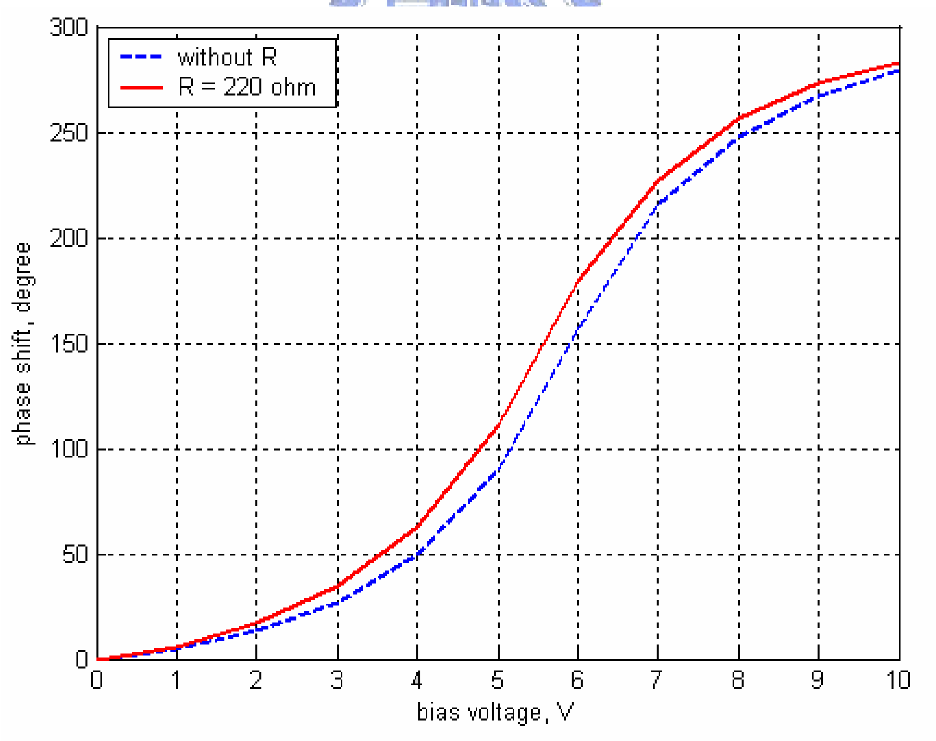

(a)

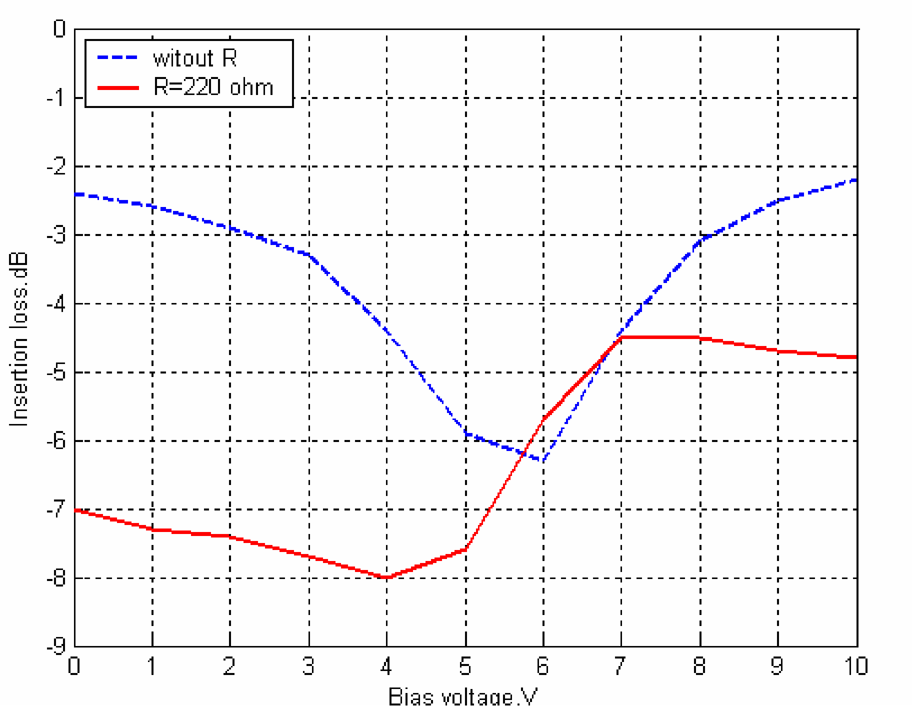

(b)

Figure 3.11: Measured results of the proposed phase shifters against bias voltage at 12.45 GHz. (a) Relative phase shift. (b) Insertion loss

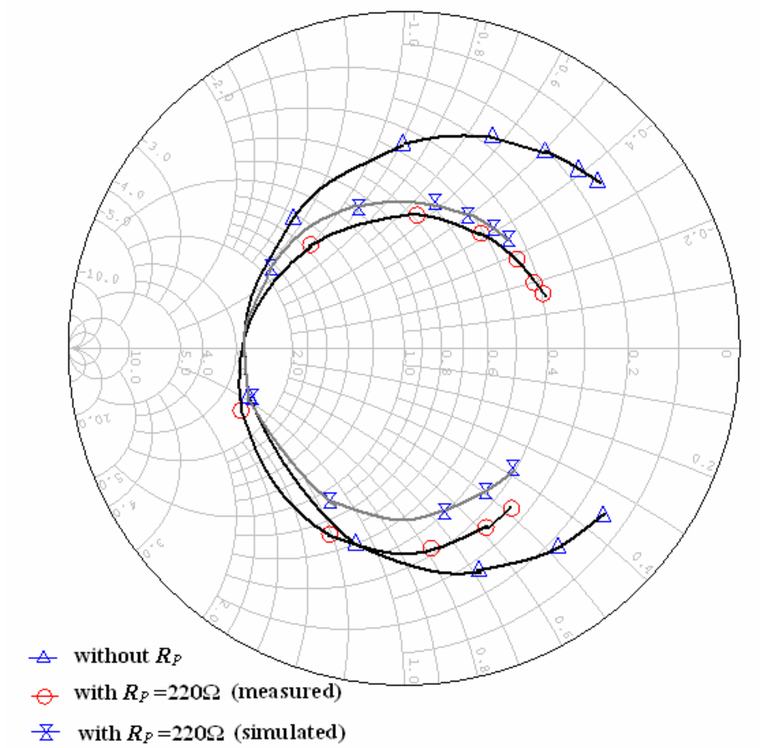

Figure 3.12: Measured S_{21} of the proposed phase shifters at 12.45 GHz.

3.4.2 Performance against Frequency

Because the frequency response is mainly determined by the 3-dB 90° hybrid coupler and the cascaded quarter-wave impedance transformers, only the case of the one without R_P is concerned. Figure 3.13 shows the measured performances such as phase shifts, insertion loss, and return loss of the phase shifters without R_P over the bandwidth of 12.2 GHz to 12.7 GHz. The Figure shows that insertion-loss variation is within $\pm$2dB, return loss is better than -12dB, and phase shift is more than 280° over 500MHz at the phase stages of bias voltage from 0V to 10V.

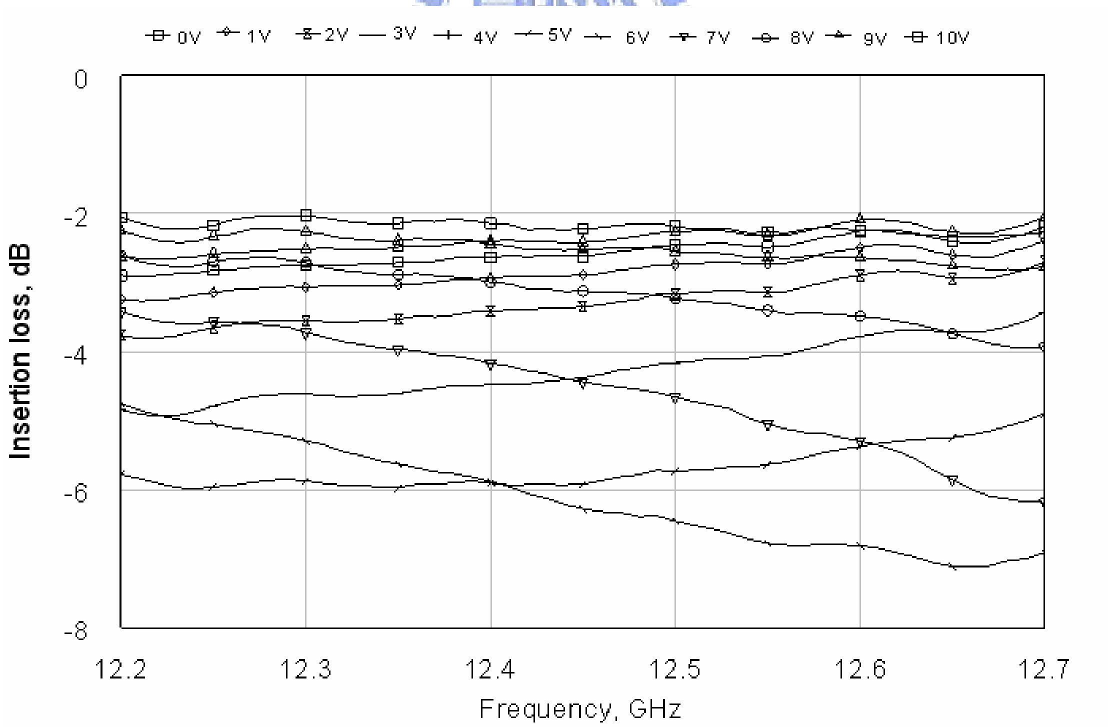

(a)

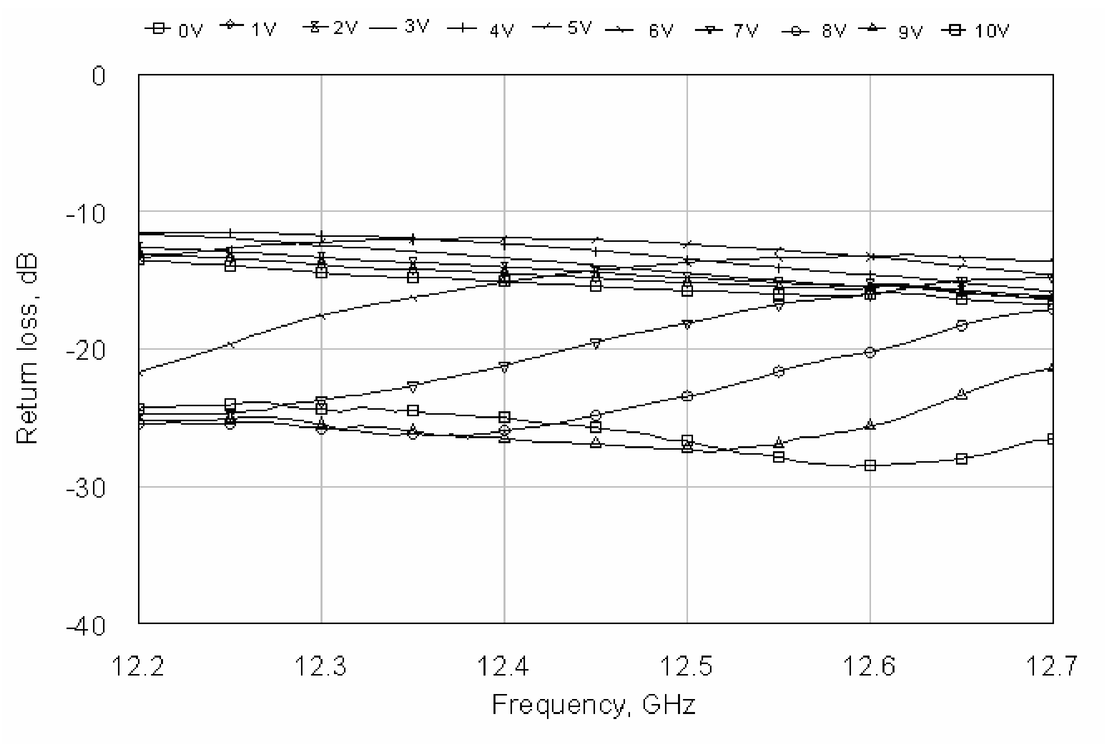

(b)

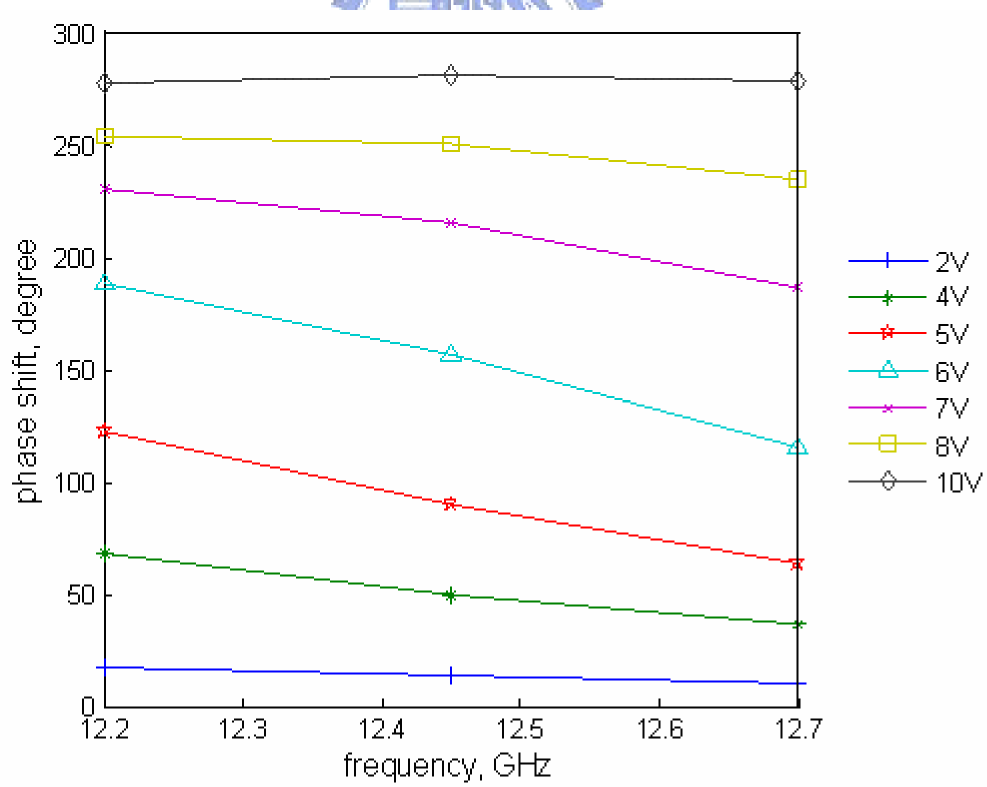

Figure 3.13: Measured frequency performance of the proposed phase shift. (a) Insertion loss. (b) Return loss. (c) Relative phase shift.

3.5 Ku Band Phased Array

3.5.1 Theory

A phased array is a group of antennas in which the relative phases of the signals feeding the antennas are varied, so the radiation pattern of the array is reinforced in the desired direction and suppressed in undesired direction. The proposed phased shifters are used in the phased array as beamformers to provide high-speed beam-steering and high directivity. As shown in Figure 3.14, the phased array is a combination of N antennas with equidistance, and the array factor (AF) is defined as

$$AF = \sum_{n=0}^{N} A_n e^{jn(\beta d \sin\theta + \alpha)} \tag{3.10}$$

where A_n represents the amplitude of the signal radiated by the n-th element; α and d represent the phase shift and distance between successive antennas, respectively. Let $\psi = \beta d \sin\theta + \alpha$, then

$$AF = \sum_{n=0}^{N} A_n e^{jn\psi} \tag{3.11}$$

We can see that the maximum energy is derived when $\psi = 0$. That is,

$$\alpha = -\beta d \sin\theta \tag{3.12}$$

Therefore, if we want to control the angle at which the maximum power is emitted or received (main beam), we only need to adjust the phase shift α of successive antennas.

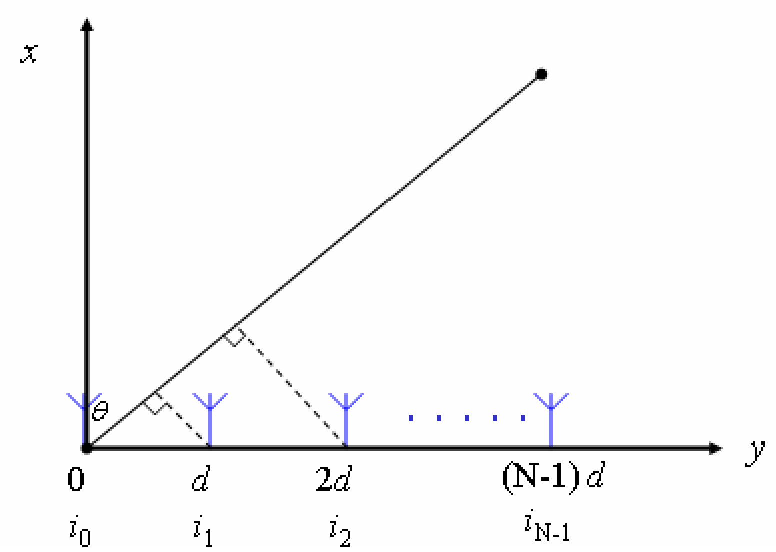

Figure 3.14: Phased array composed of N antennas with equidistance.

Now space the antennas a distance d of 1.03 λ at center frequency of 12.45 GHz. Chosen N=4, the simulated radiation patterns with different phase shift α are shown in Figure 3.15. Each element of the phased array is assumed to be omnidirectional for simplicity. It shows that for d being approximately one wavelength, there are 4 or 5 main lobes. Considering the first quadrant (left-top), the angle of the main lobe θ is 0^o, 8^o, 16^o, 30^o, 46^o, and 59^o, when phase shift α is 0^o, -50^o, -100^o, -180^o, -260^o, and -310^o, respectively. Figure 3.16 shows the relationship between α and θ at the first quadrant. It shows that the direction of main beam can be arbitrarily controlled if a full 360^o phase shifter is used.

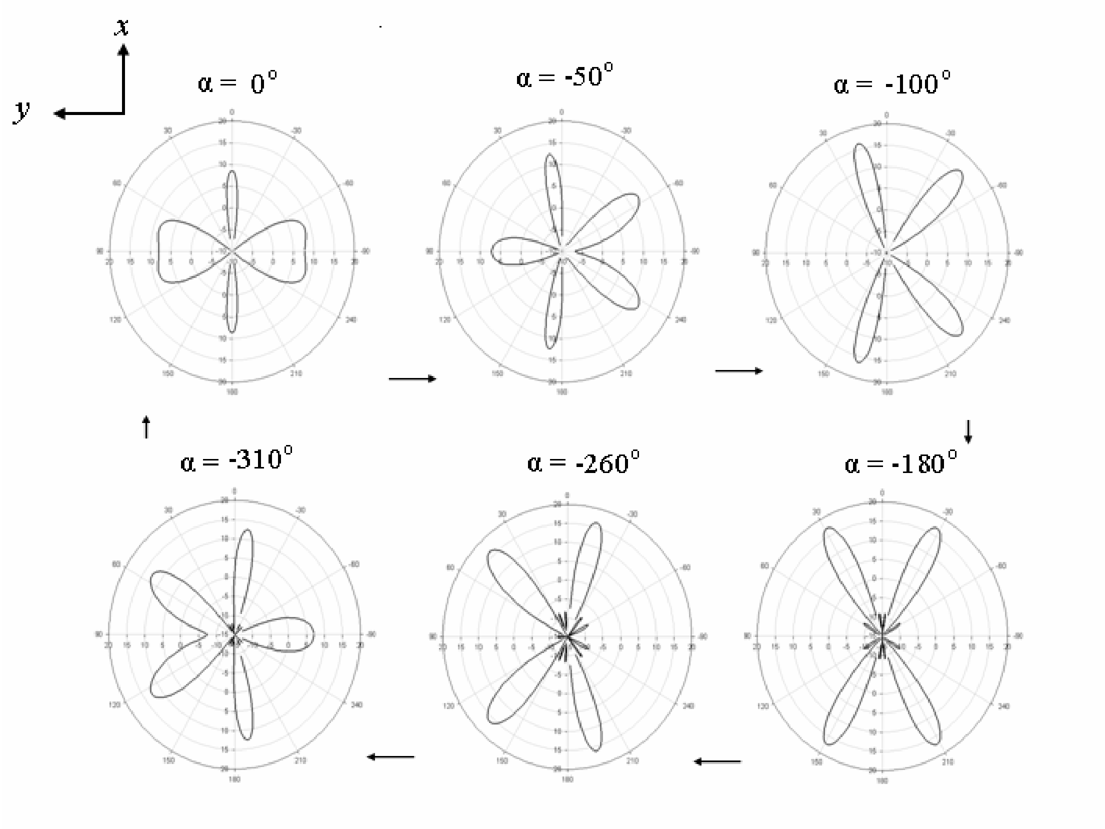

Figure 3.15: Simulated radiation pattern of 4-element phased array.

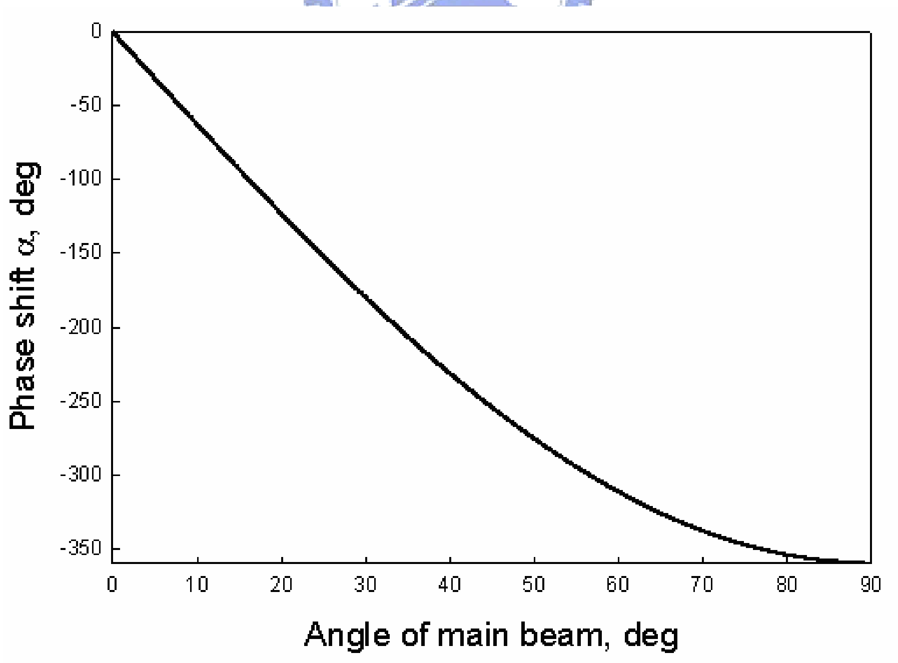

Figure 3.16: Relationship between the angle of main beam and phase shift between successive antennas.

3.5.2 Design

The structure of the proposed phased array with 4 elements is shown in Figure 3.17. The series-feed phased array is used for simplicity of control, and dipole antennas are used for omnidirectional radiation pattern. Then, the received signals are coupled to the signal path by a directional coupler. With the same control voltage of phase shifter, each phase shift between successive antennas is identical to the others. However, the phase shifters accumulate insertion loss along the path. In order to receive the same power from each antenna at the output port, a low noise amplifier is added in front of each phase shifter to compensate the insertion loss.

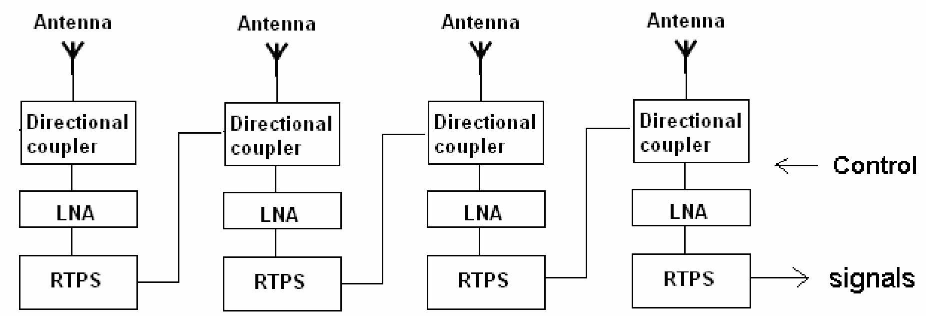

Figure 3.17: The structure of the proposed phased array. (RTPS: reflection-type phase shifter. LNA: low noise amplifier)

3.5.3 Fabrication and Measurements

The photograph of the proposed Ku band phased array is shown in Figure 3.18, in which the components of the phased array are illustrated. The phased array is designed at the center frequency of 12.45 GHz, with its size of 10×4 cm^2. Dipole antennas are chosen for omnidirectional. The directional coupler is designed with a coupling factor of -14 dB and its through port is terminated with a 50Ω resistor. The received signal is coupled to its coupled port and direct to the output port of the phased array.

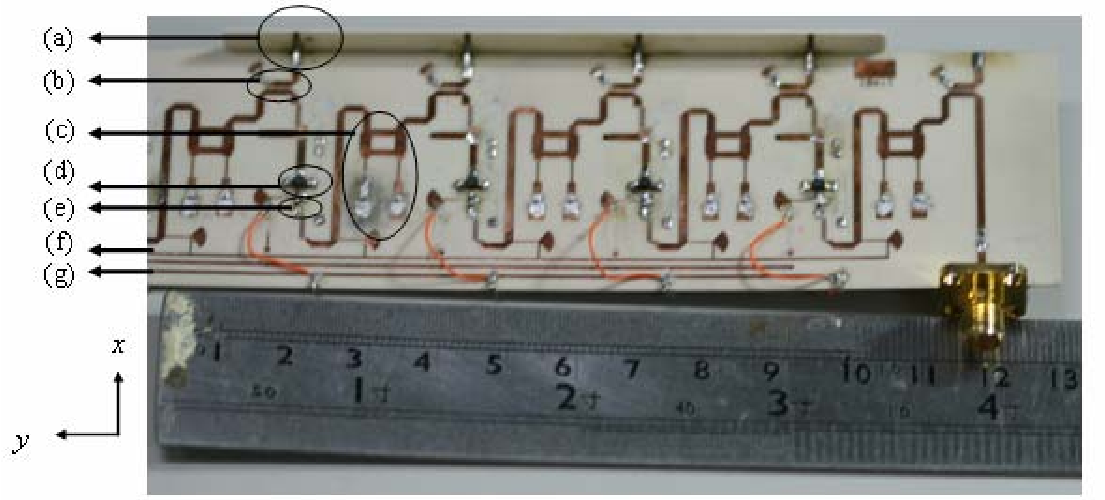

Figure 3.18: Photograph of the proposed phased array. (a) Dipole antenna. (b) Directional coupler. (c) Reflection-type phase shifter. (d) Low noise amplifier. (e) Chip resistor (100Ω). (f) Control voltage of phase shifters (0-10V). (g) LNA bias voltage (1.5V).

Figure 3.19 shows the radiation pattern of the proposed phased array against different control voltage of the phase shifter. It was measured at 12.2, 12.45, and 12.7 GHz, which is the band of broadcasting satellite service (BSS). Even if the insertion loss is compensated by LNA, the radiation gain suffers from the insertion-loss variation with control voltage of the phase shifter. The angle of main beam against control voltage is shown in Figure 3.20.

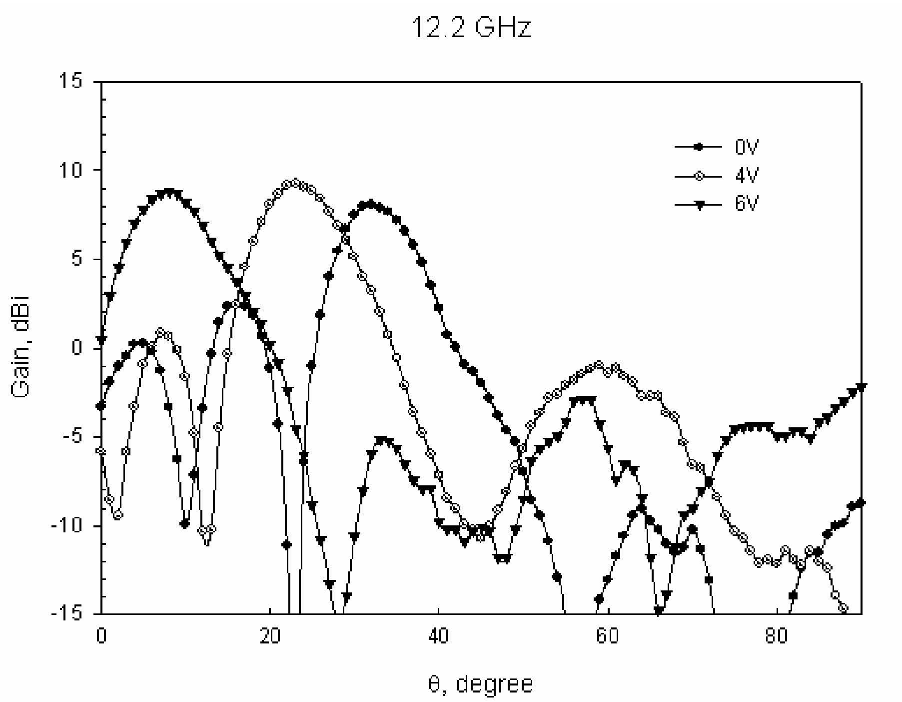

(a)

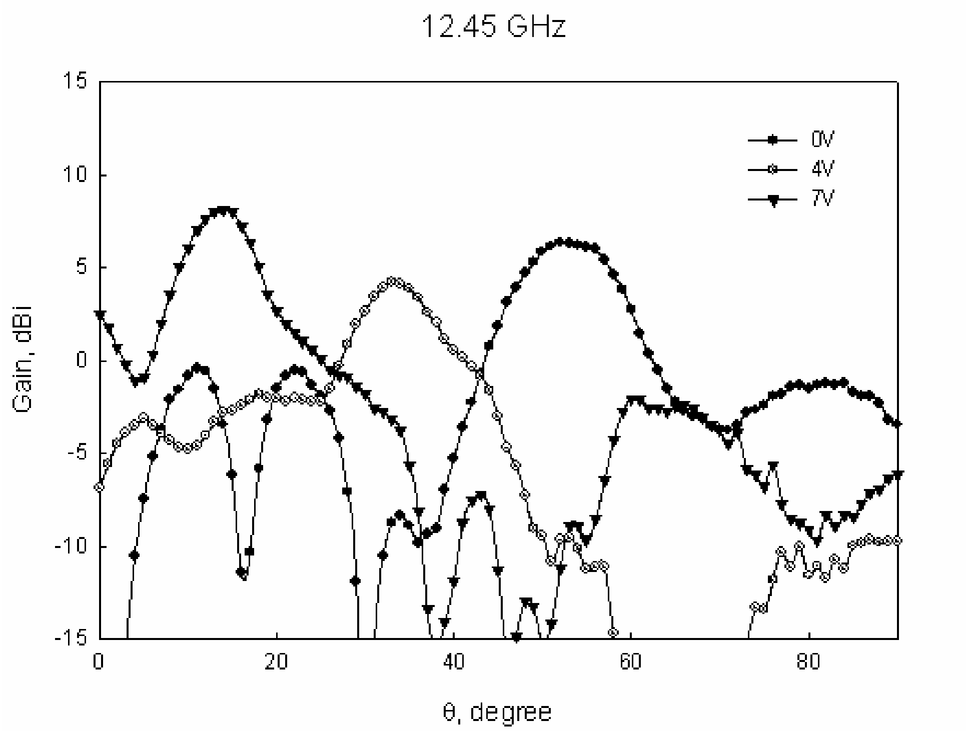

(b)

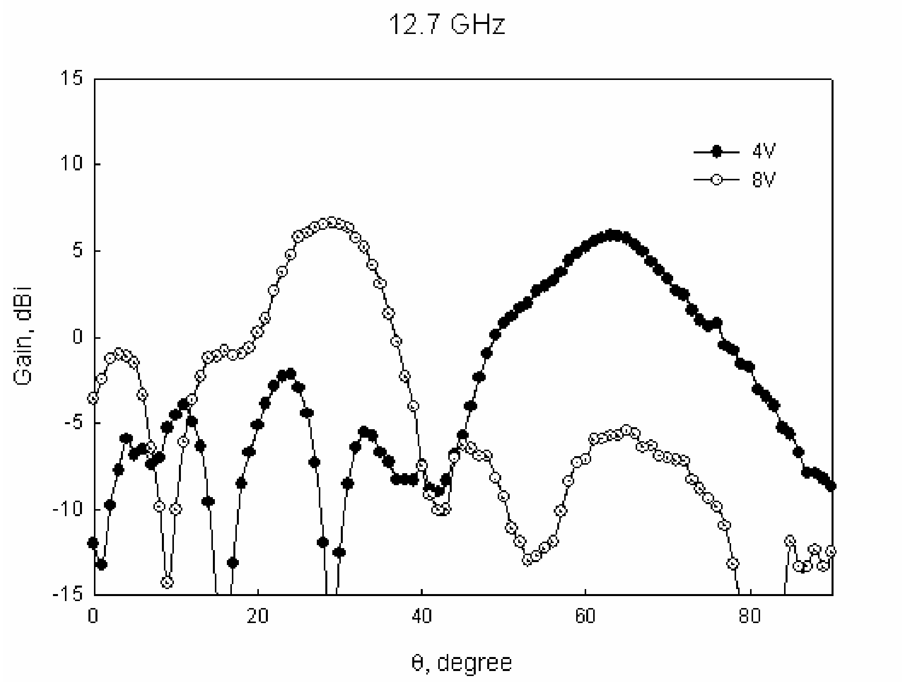

(c)

Figure 3.19: Measured radiation pattern of the proposed Ku band phased array at (a) 12.2 GHz. (b) 12.45 GHz. (c) 12.7 GHz

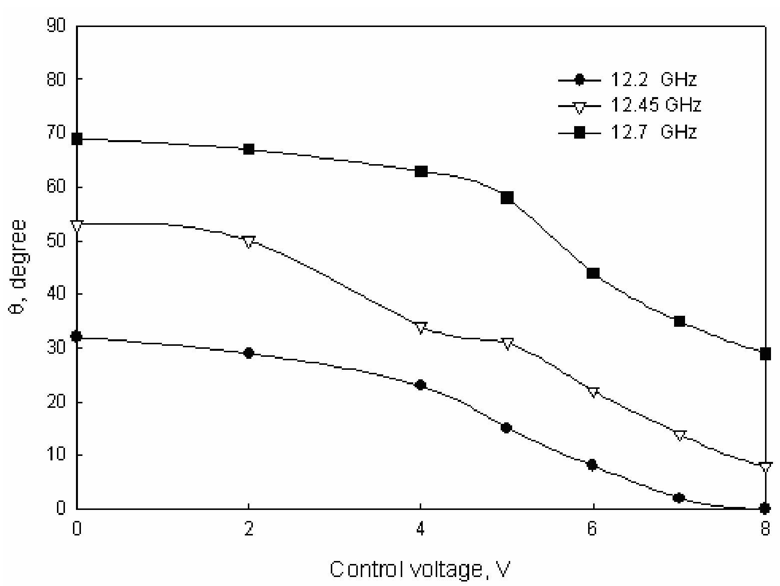

Figure 3.20: The angle of main beam against control voltage.

Chapter 4
Reduced-Size Impedance-Transforming Broadband 180^o Hybrid Ring

4.1 Introduction

The 180^o hybrid ring coupler, which is also known as a rat-race ring, is an essential component in microwave circuits, such as balanced mixers, multipliers, push-pull amplifiers and antenna feed network, etc. A conventional a rat-race ring consists of three $\lambda/4$ line sections and one $3\lambda/4$ line section. The $3\lambda/ 4$ line section works as a $\lambda/4$ line section with a phase inverter formed by a $\lambda/2$ line section. Thus, the disadvantage of the conventional rat-race ring is narrow bandwidth and large size.

Many researches [10]-[14] have attributed to make the bandwidth larger. Most of the approaches are realizing an ideal or broadband phase inverter. Replaced the $3\lambda/ 4$ line section with a short-circuited $\lambda/ 4$ coupled line section of March [10], which not only reduce size but also widen the bandwidth of the rat-race ring. However, the tight coupled line is hard to be realized. An ideal phase inverter, which is shown in Figure 4.1(a), provides perfect amplitude and phase performance. In [11], [12], the combination of coplanar waveguide (CPW) and coplanar strips (CPS) or slot lines was used in the 180° hybrid ring. In these designs, frequency independent phase inverter of the hybrid ring has been implemented by CPS direct cross-type phase inverter. Another technique to increase the bandwidth is by converting baluns into 180° hybrid ring by adding an in-phase power splitter presented in [13]. In addition to realizing the broadband phase inverter, increasing the order of circuit response may widen the bandwidth as well. In [14], a broadband Chebyshev-response rat-race ring with a $\lambda/4$ unit element at each port and an ideal phase inverter is proposed.

Many approaches [15]-[19] have been presented to reduce the size of hybrid rings. These methods include the use of folded lines [15], artificial lines [16], defected ground structure [17], lump elements [18], and others [19]. However, the above approaches are hard to achieve a wide bandwidth. In [20], both wideband and size reduction are achieved by an interdigital CPS inverter.

In this chapter, a reduced-size impedance-transforming broadband 180° hybrid ring coupler is presented. With a unit element at each port and an ideal phase inverter, which was proposed in [14], the broadband rat-race ring with a Chebyshev response of order 3 or 4 has been developed. In [21], the author modified the coupler and developed the design and optimization method of a 180° hybrid ring for Chebyshev equiripple functions including impedance transformation between the input and output ports, as shown in Figure 4.1(b). The values of the admittance Y_1, Y_2, Y_{t1}, and

Y_{t2} in Figure 4.1(b) are determined by the optimization method to synthesize a broadband rat-race ring with an impedance transforming ratio of 1:3. We replace each line section by the stepped-impedance CPS/interdigital CPS structure proposed in [20] not only to realize an ideal 180° phase inverter but also miniaturize the circuit size. A miniaturized broadband 180° hybrid ring coupler with impedance transformation of from 40Ω to 120Ω using the stepped-impedance CPS/interdigital CPS structure is realized. The circuit analysis, design procedure, simulation and measurement results are discussed in this chapter.

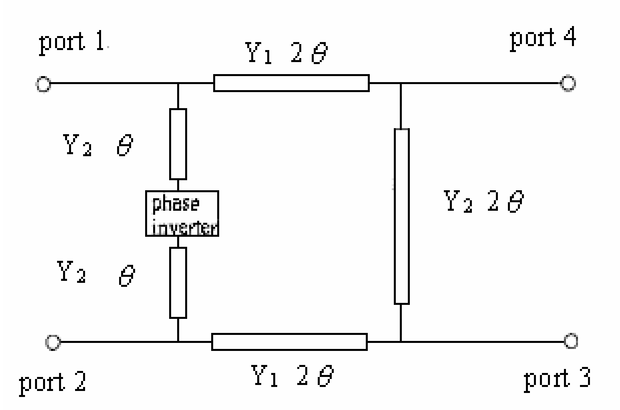

(a)

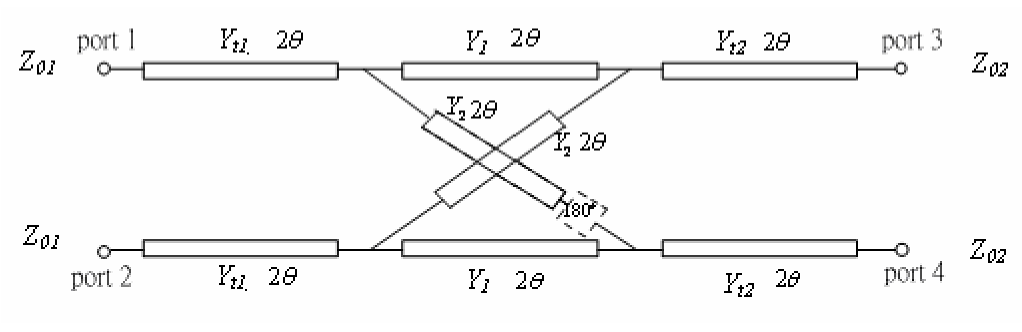

(b)

Figure 4.1: Circuit schematics of 180° hybrid ring with an ideal phase inverter. (a)

Conventional 180^o hybrid ring. (b) Proposed broadband 180^o hybrid ring with different impedance at input and output ports.

4.2 Theory

4.2.1 Conventional 180^o Hybrid Ring

The circuit schematic of an 180^o hybrid ring with an ideal phase inverter is shown in Figure 4.1(a). Instead of a conventional rat-race ring composed of three $\lambda_g/4$ and one $3\lambda_g/4$ line sections, the spacing between all adjacent ports is $\lambda_g/4$, and an ideal phase inverter is placed between two of the adjacent ports. With the use of an ideal phase shifter, the bandwidth of 180^o hybrid ring is further increased. Even- and odd-mode equivalent circuits of the hybrid ring are shown in Figure 4.2(a) and (b).

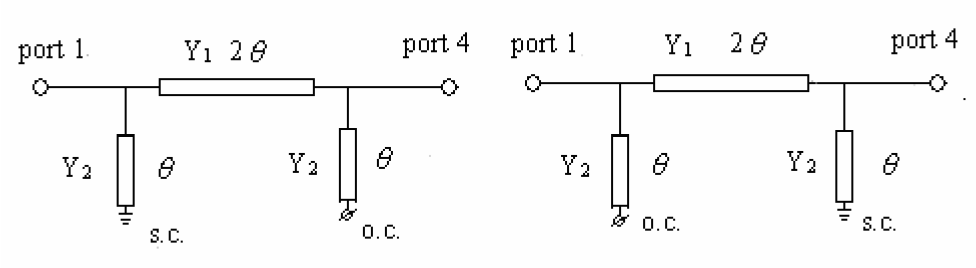

(a) (b)

Figure 4.2: (b) Even- and (b) Odd-mode equivalent circuits of the 180^o hybrid ring with an ideal phase inverter.

The ABCD matrices for the even- and odd-mode circuits are

$$\begin{bmatrix} A_e & B_e \\ C_e & D_e \end{bmatrix} = \begin{bmatrix} 1 & 0 \\ jY_2 \tan\theta & 1 \end{bmatrix} \begin{bmatrix} \cos 2\theta & jZ_1 \sin 2\theta \\ jY_1 \sin 2\theta & \cos 2\theta \end{bmatrix} \begin{bmatrix} 1 & 0 \\ -jY_2 \cot\theta & 1 \end{bmatrix} \tag{4.1}$$

$$\begin{bmatrix} A_o & B_o \\ C_o & D_o \end{bmatrix} = \begin{bmatrix} 1 & 0 \\ -jY_2 \cot\theta & 1 \end{bmatrix} \begin{bmatrix} \cos 2\theta & jZ_1 \sin 2\theta \\ jY_1 \sin 2\theta & \cos 2\theta \end{bmatrix} \begin{bmatrix} 1 & 0 \\ jY_2 \tan\theta & 1 \end{bmatrix} \tag{4.2}$$

where Y_1 and Y_2 are normalized admittance of the hybrid ring, which are normalized to port impedance Z_0. Let θ=45° at the center frequency, then

$$\begin{bmatrix} A_e & B_e \\ C_e & D_e \end{bmatrix}_{\theta=45^o} = \begin{bmatrix} 1 & 0 \\ jY_2 & 1 \end{bmatrix} \begin{bmatrix} 0 & jZ_1 \\ jY_1 & 0 \end{bmatrix} \begin{bmatrix} 1 & 0 \\ -jY_2 & 1 \end{bmatrix} = \begin{bmatrix} \frac{Y_2}{Y_1} & j\frac{1}{Y_1} \\ j\frac{Y_1^2+Y_2^2}{Y_1} & -\frac{Y_2}{Y_1} \end{bmatrix} = \begin{bmatrix} A & B \\ C & D \end{bmatrix} \tag{4.3}$$

$$\begin{bmatrix} A_o & B_o \\ C_o & D_o \end{bmatrix}_{\theta=45^o} = \begin{bmatrix} 1 & 0 \\ -jY_2 & 1 \end{bmatrix} \begin{bmatrix} 0 & jZ_1 \\ jY_1 & 0 \end{bmatrix} \begin{bmatrix} 1 & 0 \\ jY_2 & 1 \end{bmatrix} = \begin{bmatrix} -\frac{Y_2}{Y_1} & j\frac{1}{Y_1} \\ j\frac{Y_1^2+Y_2^2}{Y_1} & \frac{Y_2}{Y_1} \end{bmatrix} = \begin{bmatrix} D & B \\ C & A \end{bmatrix} \tag{4.4}$$

The S parameters of the four-port network are

$$S_{11} = S_{22} = \frac{B-C}{A+B+C+D} = \Gamma \tag{4.5a}$$

$$S_{21} = S_{12} = \frac{2}{A+B+C+D} = \mathrm{T} \tag{4.5b}$$

$$S_{31} = S_{13} = 0 \tag{4.5c}$$

$$S_{41} = \frac{A-D}{A+B+C+D} = \frac{2(Y_1/Y_2)}{A+B+C+D} \tag{4.5d}$$

$$S_{32} = \frac{D-A}{A+B+C+D} = \frac{-2(Y_1/Y_2)}{A+B+C+D} \tag{4.5e}$$

The output power division ratio is

$$R = \frac{|S_{41}|^2}{|S_{21}|^2} = \frac{|S_{32}|^2}{|S_{12}|^2} = \left(\frac{Y_1}{Y_2}\right)^2 \tag{4.6}$$

By (4.5) and (4.6), the normalized admittance Y_1 and Y_2 are related to return loss and power division. The scattering matrix of an 180° hybrid ring makes it useful in many applications. For example, if an 180^o hybrid ring is designed for equal power division, that is, $Y_1 = Y_2$, it is equivalent to an in-phase power divider and a balun. When an input signal is incident at port 1 (delta port), the balun provides 180^o out-of-phase equal power division between port 2 and 4, and no power reaches port 3. On the other hand, when power is incident at port 3 (sum port), the power divider provides in-phase power division between port 2 and 4, and no power reaches port 1.

4.2.2 Impedance-Transforming Broadband 180^o Hybrid Ring

The circuit schematic of the proposed broadband Chebyshev response 180^o hybrid ring with impedance transforming between input and output is shown in Figure 4.1(b). Instead of the conventional 180^o hybrid ring with an ideal phase inverter mentioned in the previous section, the proposed 180^o hybrid ring comprises a reconfigured hybrid ring [22] and an additional λ/4 unit element at each input and output (I/O) port. With the reconfigured hybrid ring shown in Figure 4.3(a), the input/output ports are on the same side so that it is easier to analysis the proposed circuit, which is a cascade of a single ring and unit elements. Based on even-odd mode analysis and the scattering matrix of interconnected networks, the circuit analysis of the proposed 180^o hybrid ring is separated into two parts, as shown in Figure 4.3(a) and (b). The first part is the reconfigured 180° hybrid ring with an ideal phase inverter and the second part is one pair of unit elements with the same characteristic impedance at the same side. The whole circuit is a cascading of a single-section hybrid ring and two pairs of unit elements. After the circuit analysis of each 4-port network, we can derive the scattering matrix of the overall network.

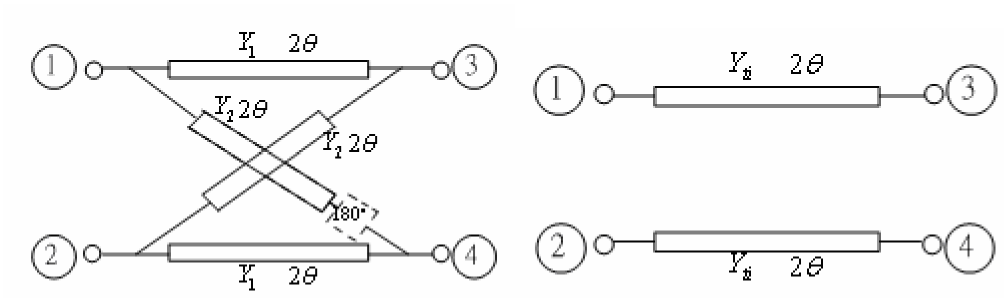

(a) (b)

Figure 4.3: Circuit schematics of (a) the reconfigured hybrid ring with an ideal phase inverter (b) one pair of unit elements with the same impedance at the same side.

Consider the single-section hybrid ring in Figure 4.3(a). Using the even-odd mode analysis, the ABCD matrices are given by

$$\begin{bmatrix} A_e & B_e \\ C_e & D_e \end{bmatrix} = \frac{1}{\left(1-t^2\right)} \begin{bmatrix} A_1(t^2) & tB_0(t^2) \\ \frac{1}{t}C_2(t^2) & D_1(t^2) \end{bmatrix} = \begin{bmatrix} A & B \\ C & D \end{bmatrix} \tag{4.7}$$

$$\begin{bmatrix} A_o & B_o \\ C_o & D_o \end{bmatrix} = \begin{bmatrix} D & B \\ C & A \end{bmatrix} \tag{4.8}$$

where $t = j\tan\theta$ and A, B, C, D are the polynomials of t^2, where the subscripts denotes the order of polynomials. Therefore, the S-parameters of the single-section hybrid ring are

$$S_{11s} = S_{22s} = \frac{B/Z_0 - CZ_0}{A + B/Z_0 + CZ_0 + D} \tag{4.9a}$$

$$S_{21s} = S_{12s} = 0 \tag{4.9b}$$

$$S_{31s} = S_{42s} = \frac{2}{A + B/Z_0 + CZ_0 + D} \tag{4.9c}$$

$$S_{32s} = S_{23s} = \frac{-A + D}{A + B/Z_0 + CZ_0 + D} \tag{4.9d}$$

$$S_{41s} = S_{41s} = \frac{A - D}{A + B/Z_0 + CZ_0 + D} \tag{4.9e}$$

In order to apply the optimization method, the scattering matrix is formulated at N discrete frequencies. The scattering matrix of the single-section hybrid ring at the kth frequency is

$$[S]_{s,k} = \begin{bmatrix} S_{11s,k} & 0 & S_{31s,k} & S_{41s,k} \\ 0 & S_{22s,k} & S_{32s,k} & S_{31s,k} \\ S_{31s,k} & S_{32s,k} & S_{22s,k} & 0 \\ S_{41s,k} & S_{31s,k} & 0 & S_{11s,k} \end{bmatrix} = \begin{bmatrix} [S_{CC}] & [S_{CD}] \\ [S_{DC}] & [S_{DD}] \end{bmatrix} \tag{4.10}$$

where $[S_{CC}]$, $[S_{DC}]$, $[S_{CD}]$, and $[S_{DD}]$ are the matrices of order 2×2.

For a single unit element with a characteristic admittance value of Y_{ti} and an electrical length of 2θ, its ABCD matrix is

$$\begin{bmatrix} A_u & B_u \\ C_u & D_u \end{bmatrix} = \frac{1}{1-t^2} \begin{bmatrix} 1+t^2 & \frac{2t}{Y_{ti}} \\ 2Y_{ti}t & 1+t^2 \end{bmatrix} \tag{4.11}$$

Thus, the scattering matrix of the ith pair of unit elements shown in Figure 4.3 (b) at the kth frequency in the bandwidth is

$$[S]_{ui,k}=\begin{bmatrix} S_{11ui,k} & 0 & S_{13ui,k} & 0 \\ 0 & S_{11ui,k} & 0 & S_{13ui,k} \\ S_{13ui,k} & 0 & S_{11ui,k} & 0 \\ 0 & S_{13ui,k} & 0 & S_{11ui,k} \end{bmatrix}=\begin{bmatrix} [S_{AA}] & [S_{AB}] \\ [S_{AB}] & [S_{AA}] \end{bmatrix} \tag{4.12}$$

where $S_{13ui,k}=\dfrac{B_{ui}/Z_0-C_{ui}Z_0}{2A_{ui}+B_{ui}/Z_0+C_{ui}Z_0}$, $S_{13ui,k}=\dfrac{2}{2A_{ui}+B_{ui}/Z_0+C_{ui}Z_0}$, and $[S_{AA}]$, $[S_{AB}]$, $[S_{BA}]$, and $[S_{BB}]$ are the matrices of order 2×2.

The scattering matrix of the interconnection network can be derived by using matrix algebra [23]. It follows that the scattering matrix S_R' of the interconnection of a pair of unit elements and a single-section hybrid ring is

$$[S_R']=\begin{bmatrix} [S_1] & [S_2] \\ [S_3] & [S_4] \end{bmatrix} \tag{4.13}$$

where $[S_1]$, $[S_2]$, $[S_3]$, $[S_4]$ are given by

$$[S_1]=[S_{AA}]+[S_{AB}]([U]-[S_{CC}][S_{BB}])^{-1}[S_{CC}][S_{BA}]$$

$$[S_2]=[S_{AB}]([U]-[S_{CC}][S_{BB}])^{-1}[S_{CD}]$$

$$[S_3]=[S_{DC}]([U]-[S_{BB}][S_{CC}])^{-1}[S_{BA}]$$

$$[S_4]=[S_{DD}]+[S_{DC}]([U]-[S_{BB}][S_{CC}])^{-1}[S_{BB}][S_{CD}] \tag{4.14}$$

where $[U]$ represents the 2×2 identity matrix. After the scattering matrix S_R' is derived, we cascade the network with the other pair of unit elements on the opposite side and use the same method to derive the scattering matrix S_R of the overall network as shown in Figure 4.1(b).

After deriving the scattering matrix S_R, we consider changing the port impedance of the 180^o hybrid ring. The detailed derivation of changing circuit impedance is given in [24]. For the hybrid ring to transform from source (port 1 and 2) impedances of Z_{01} to load (port 3 and 4) impedances of Z_{02}, the scattering matrix S_C is expressed in terms of the original scattering matrix S_R and the reflection coefficient r_n of Z_{0n} with respect to Z_0.

$$[S_C] = [A]^{-1}\left([S_R] - [\Gamma]^{+}\right)\left([I] - [\Gamma][S]\right)^{-1}[A]^{+} \tag{4.15}$$

where + indicates the complex conjugate transposed matrix, $[I]$ is a 2×2 identity matrix, $[A]$ is a diagonal matrix of which the nth diagonal component A_n is given by

$$A_n = \frac{1 - r_n^*}{|1 - r_n|}\sqrt{|1 - r_n r_n^*|} \tag{4.16}$$

and $[\Gamma]$ is a diagonal matrix of which the nth diagonal component r_n is given by

$$r_n = \frac{Z'_{0n} - Z_{0n}}{Z'_{0n} + Z_{0n}^*} \tag{4.17}$$

4.2.3 Cost Function and Optimization

For an 180^o hybrid ring, the input power at port 1 is divided between output ports (port 3 and 4), while the isolation at port 2 should be as high as possible. Similarly, the input power at port 2 is divided between output ports, while the isolation at port 1 should be as high as possible. Thus, the cost function in terms of the scattering parameters of the proposed circuit is designed as

$$
\begin{aligned}
f = & wt1\sum_k\left[P_{11,k}-P_{RL,k}\right]^2 + wt2\sum_k\left[P_{31,k}-P_{CP,k}\right]^2 + wt3\sum_k\left[P_{41,k}-(P_{tot,k}-P_{RL,k}-P_{CP,k})\right]^2 \\
& + wt4\sum_k\left[P_{21,k}\right]^2 + wt1\sum_k\left[P_{22,k}-P_{RL,k}\right]^2 + wt2\sum_k\left[P_{42,k}-P_{CP,k}\right]^2 \\
& + wt3\sum_k\left[P_{32,k}-(P_{tot,k}-P_{RL,k}-P_{CP,k})\right]^2 + wt4\sum_k\left[P_{12,k}\right]^2
\end{aligned}
\tag{4.18}
$$

where the subscript k indicates the kth discrete frequency in the bandwidth and

$$P_{11,k}=\frac{|S_{11,k}|^2}{2Z_S},\quad P_{21,k}=\frac{|S_{21,k}|^2}{2Z_S},\quad P_{31,k}=\frac{|S_{31,k}|^2}{2Z_L},\quad P_{41,k}=\frac{|S_{41,k}|^2}{2Z_L},$$

$$P_{12,k}=\frac{|S_{12,k}|^2}{2Z_S},\quad P_{22,k}=\frac{|S_{22,k}|^2}{2Z_S},\quad P_{32,k}=\frac{|S_{32,k}|^2}{2Z_L},\quad P_{42,k}=\frac{|S_{42,k}|^2}{2Z_L},$$

$$P_{tot,k}=P_{11,k}+P_{21,k}+P_{31,k}+P_{41,k}$$

$$|S_{11,k}|^2+|S_{21,k}|^2+|S_{31,k}|^2+|S_{41,k}|^2=1,\quad |S_{12,k}|^2+|S_{22,k}|^2+|S_{32,k}|^2+|S_{42,k}|^2=1$$

The Chebyshev equiripple response described in [15] has the form as shown in

$$P_L=1+h^2\cdot\left\{\frac{\left(1+\sqrt{1-x_c^2}\right)T_n(x/x_c)-\left(1-\sqrt{1-x_c^2}\right)T_{n-2}(x/x_c)}{2\sqrt{1-x^2}}\right\}^2 \tag{4.19}$$

where $x=\cos 2\theta$, $x_c=\cos 2\theta_c$, and h is the parameter to control the ripple level. Applying this function to the insertion loss function and through the optimization, we can derive the circuit parameters Y_1, Y_2, Y_{t1}, and Y_{t2}. Actually, by the cost function and optimization method, the hybrid ring can be optimized to an arbitrary function.

To verify the theory, we consider an 180° hybrid ring with equal power division, 15dB return loss, and an impedance-transforming ratio of 1:3 (40Ω to 120Ω). In this case, Z_{01} = 40Ω and Z_{02} = 120Ω. We used the optimization method and obtain the characteristic impedance of line sections with Z_{t1} = 43.5Ω, Z_{t2} = 71.2Ω, and Z_1=Z_2 = 63.2Ω. The simulated frequency response of the 180° hybrid ring at center frequency of 3GHz is shown in Figure 4.4. It is shown that the response is order three and the bandwidth of 15dB return-loss is 100%.

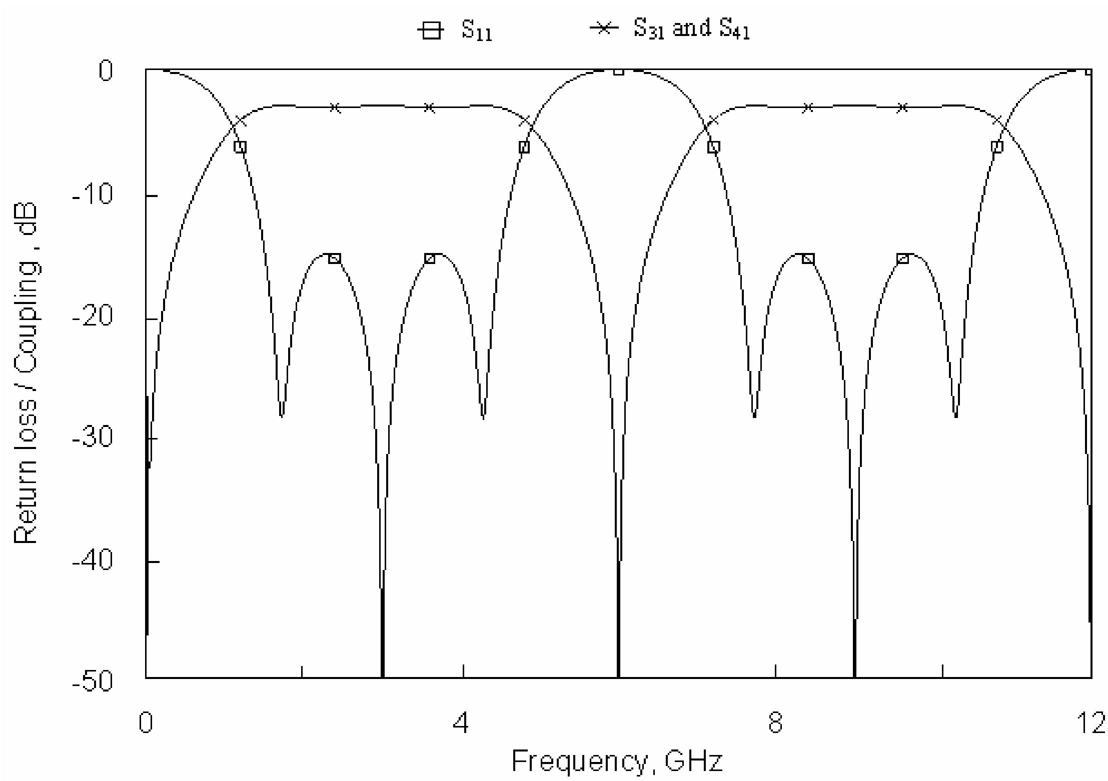

Figure 4.4: Simulated frequency response of the proposed impedance-transforming broadband 180° hybrid ring.

4.2.4 Stepped-Impedance Structure

It is well-known that the λ/4 transmission line, which is the basic building block of hybrid ring, can be replaced by the stepped-impedance structure in Figure 4.5(b).

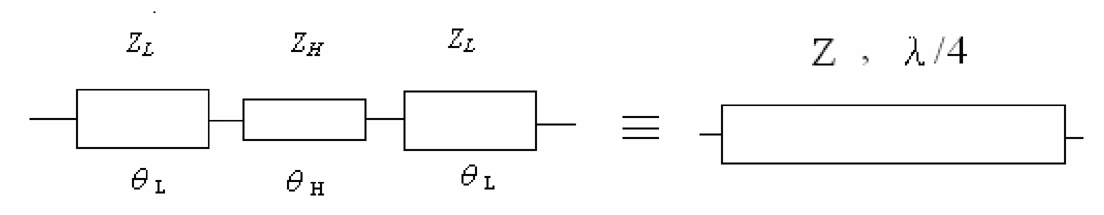

Figure 4.5: Stepped-impedance structure equivalent to a λ/4 transmission line.

With the stepped-impedance structure, it can not only remove the first several spurious signals but also reduce the size of the circuit. Equate the ABCD matrices of the λ/4 transmission line and stepped-impedance circuit as,

$$\begin{bmatrix} A & B \\ C & D \end{bmatrix} = \begin{bmatrix} 0 & jZ \\ j\frac{1}{Z} & 0 \end{bmatrix}$$
$$= \begin{bmatrix} \cos\theta_L & jZ_L \sin\theta_L \\ jY_L \sin\theta_L & \cos\theta_L \end{bmatrix} \begin{bmatrix} \cos\theta_H & jZ_H \sin\theta_H \\ jY_H \sin\theta_H & \cos\theta_H \end{bmatrix} \begin{bmatrix} \cos\theta_L & jZ_L \sin\theta_L \\ jY_L \sin\theta_L & \cos\theta_L \end{bmatrix} \tag{4.20}$$

where Z_H, Z_L are the characteristic impedance of the stepped-impedance transmission lines and θ_H, θ_L are the electrical length, respectively. For a given characteristic impedance of Z_H and Z_L, the initial values of θ_H and θ_L are derived by solving the equation numerically. Thus, given the characteristic impedance of each λ/4 line section of the proposed impedance-transforming broadband 180° hybrid ring, the parameters of the stepped-impedance structure are listed in Table 4.1.

To verify the stepped-impedance structure, the simulated frequency response of the proposed stepped-impedance impedance-transforming broadband 180° hybrid ring is shown in Figure 4.6. Ideal transmission lines and an ideal phase inverter are used for circuit simulation. The bandwidth of stepped-impedance hybrid ring is a little narrower than the λ/4 structure.

Table 4.1 Parameters of the proposed 180° hybrid ring

	$Z_H(\Omega)$	$Z_L(\Omega)$	θ_H(deg)	θ_L(deg)
λ/4, $Z_1 = 63.2\Omega$	175	22	17	17
λ/4, $Z_{t1} = 43.5\Omega$	175	22	9.2	19.9
λ/4, $Z_{t2} = 71.2\Omega$	175	22	21.1	14.6

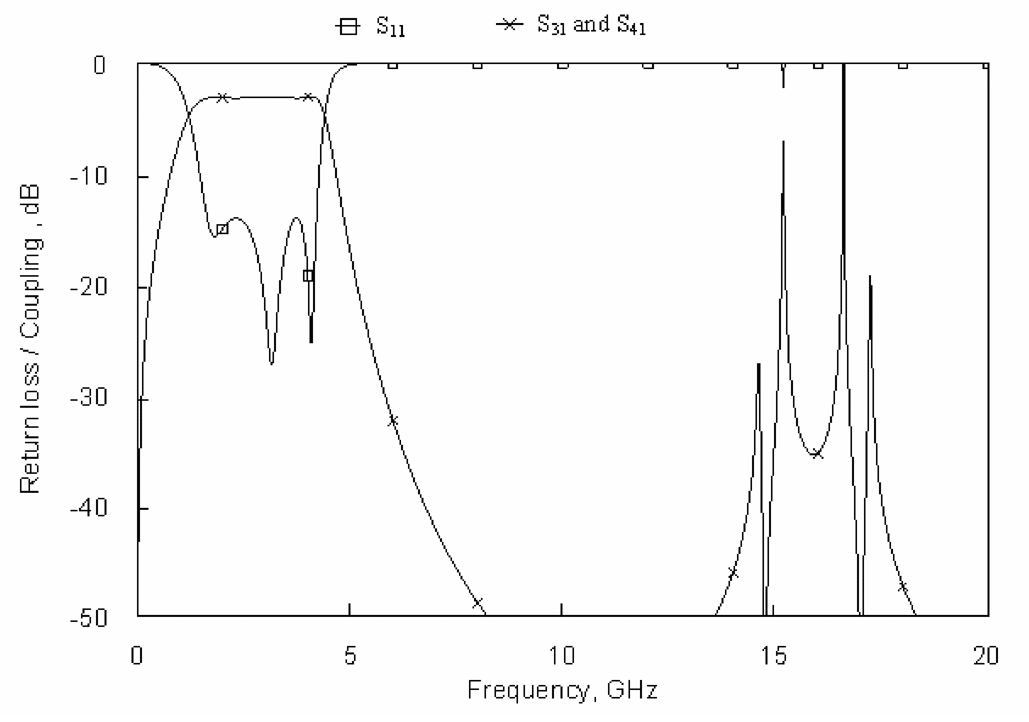

Figure 4.6: Simulated frequency response of the proposed stepped-impedance impedance-transforming broadband 180° hybrid ring using ideal transmission lines.

4.2.5 Hybrid CPS/Interdigital CPS Structure

It is well-known that for the stepped-impedance structure, size reduction is related to the impedance ratio. Larger impedance ratio is required for smaller size. In order to realize the high/low impedance at the same time, hybrid CPS/interdigital CPS structure proposed in [20] is used for the realization of the stepped-impedance transmission line. The cross sectional view of the interdigital CPS structure is shown in Figure 4.7, where W and S represent the line width and gap width of the interdigital CPS and N is the number of the CPS strip pair. It is easy to achieve high impedance for conventional CPS with large S and small W, and low impedance can be realized by interdigital CPS with small S, large W, and large N. In our design, the parameters of the hybrid CPS/interdigital CPS are listed in Table 4.2.

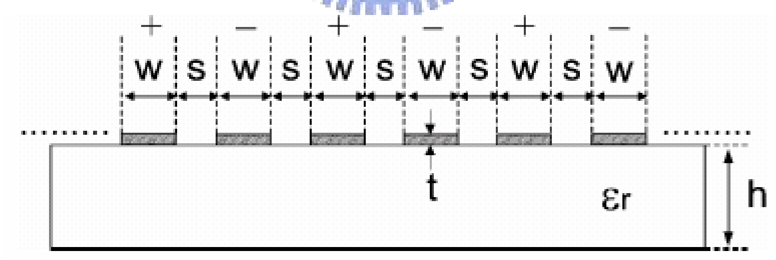

Figure 4.7: The cross section view of the interdigital CPS structure proposed in [20].

Table 4.2 Parameters of the hybrid CPS/interdigital CPS

	W (mil)	S (mil)	N	Z (Ω)
Interdigital CPS	4	1.6	3	22
CPS	4	24	1	175

Besides the realization of extreme high/low impedance of the stepped-impedance structure, there is another advantage for an 180^{o} hybrid ring using the hybrid CPS/ interdigital CPS structure. An nearly ideal 180^{o} phase inverter can be implemented in the λ/4 line section without changing its physical length. The layouts of the λ/4 line section and the one with an 180^{o} phase inverter using hybrid CPS/interdigital CPS structure are shown in Figure 4.8(a) and (b).

(a)

(b)

Figure 4.8: The layouts of the λ/4 line section using hybrid CPS/interdigital CPS structure proposed in [20] (a) λ/4 line section. (b) λ/4 line section with an 180^{o} phase inverter.

4.3 Design Procedure and Simulation

4.3.1 Design Procedure

The design procedure of the proposed stepped-impedance impedance-transforming broadband 180^{o} hybrid ring is as the following steps:

Step 1) Determine the specification such as return loss and impedance-transforming ratio of the 180^o hybrid ring. Then, derive the parameters Z_{t1}, Z_{t2}, Z_1, and Z_2 of the prototype of proposed 180^o hybrid ring in Figure 4.1(b) by the optimization method.

Step 2) Replace each λ/4 transmission line section of the stepped-impedance structure. For a given characteristic impedance of Z_H and Z_L, we can derive θ_H and θ_L by solving equation (4.20) numerically.

Step 3) Implement the stepped-impedance structure by hybrid CPS/interdigital CPS structure. The parameters θ_H and θ_L, which are initial values of the hybrid ring, are fine-tuned to optimize the performance of the circuit by EM simulation.

4.3.2 EM Simulation

The proposed stepped-impedance impedance-transforming broadband 180^o hybrid ring is designed at 3 GHz, with equal power division, 15dB return loss, and an impedance-transforming ratio of 1:3 (40Ω to 120Ω). The circuit is realized on a 15-mil Al_2O_3 substrate with a dielectric constant of 9.8. The simulation is done by Sonnet. Figure 4.9(a) and (b) show the layout of the proposed circuit. The design parameters and physical dimensions are listed in Table 4.2 and Table 4.3. The diameter of the bonding wires is set to be 1 mil.

In Figure 4.9(a), it is shown that the discontinuity effect of three junctions needs to be concerned so that the length of each CPS/interdigital CPS is different from the initial value. These discontinuities are the T junctions, the hybrid CPS/interdigital CPS junctions, and the CPW/interdigital CPS junctions. Note that instead of the designed port impedance of 40Ω or 120Ω, a CPW with impedance of 50Ω is connected to the interdigital CPS at each I/O port. This is because the network analyzer for measurement is based on system impedance of 50Ω and probing with CPW. Thus, the reference plane is de-embedded to the interconnection of the CPW/interdigital CPS junctions, as shown in the top-right corner of Figure 4.9(a).

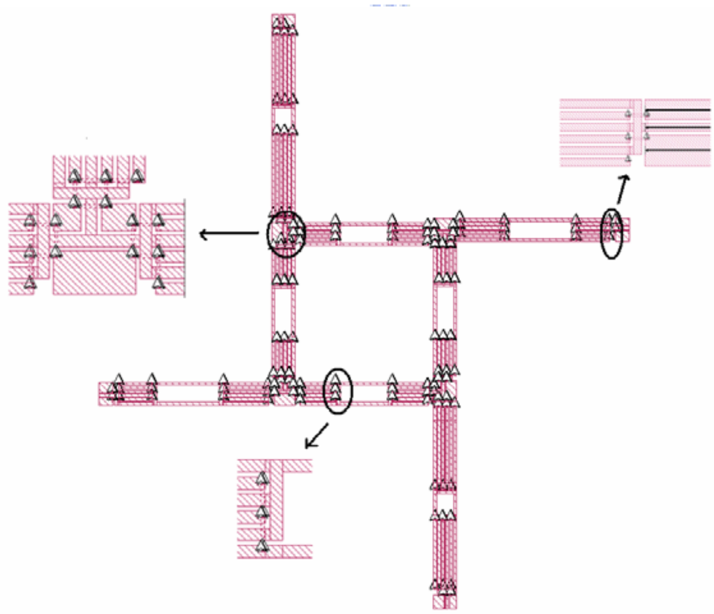

(a)

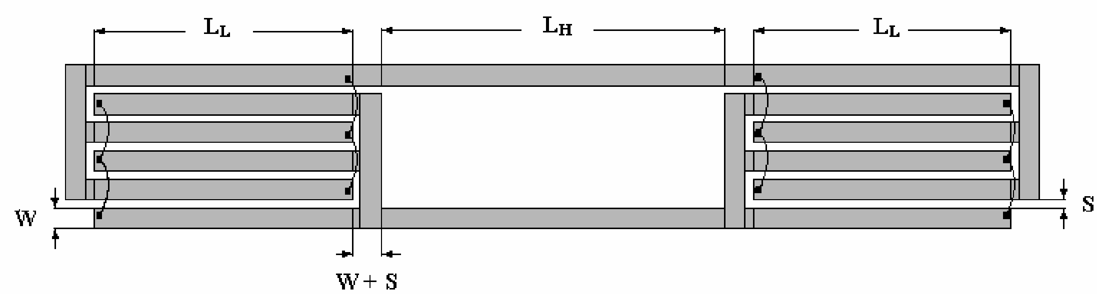

(b)

Figure 4.9: The circuit layout of the proposed stepped-impedance impedance-transforming broadband 180° hybrid ring. (a) Total circuit. (b) λ/4 line section using hybrid CPS/interdigital CPS

Table 4.3 Parameters and physical dimensions of the proposed stepped-impedance impedance-transforming broadband 180° hybrid ring.

	$Z_H(\Omega)$	$Z_L(\Omega)$	θ_H(deg)	θ_L(deg)	L_H (mil)	L_L (mil)
λ/4, $Z_1 = 63.2\Omega$	175	22	17	17	67.4	50.6
λ/4, $Z_{t1} = 43.5\Omega$	175	22	9.2	19.9	30	107.4
λ/4, $Z_{t2} = 71.2\Omega$	175	22	21.1	14.6	87.4	53.8

The bandwidth is designed as 100% from 1.5 to 2.5GHz. Figure 4.10(a) and (b) show the simulated return loss and coupling of the proposed impedance-transforming 180° hybrid ring. The amplitude balance of the coupling parameters S_{31} and S_{41} (S_{32} and S_{42}) are perfect, and the return loss is better that 10dB from 1.49 to 4.49GHz in the passband. Figure 4.11 shows the return loss for all the ports of the proposed 180° hybrid ring. It is shown that the return loss for each port in the passband is better than 10dB so that the input and output ports are matched to 40Ω and 120Ω, respectively. The simulated broadband performance of the 180° hybrid ring is shown in Figure 4.12.

Compared to the frequency response of the 180° hybrid ring without stepped-impedance in Figure 4.4, it shows no spurious S_{31} and S_{41} passband up to 12GHz.

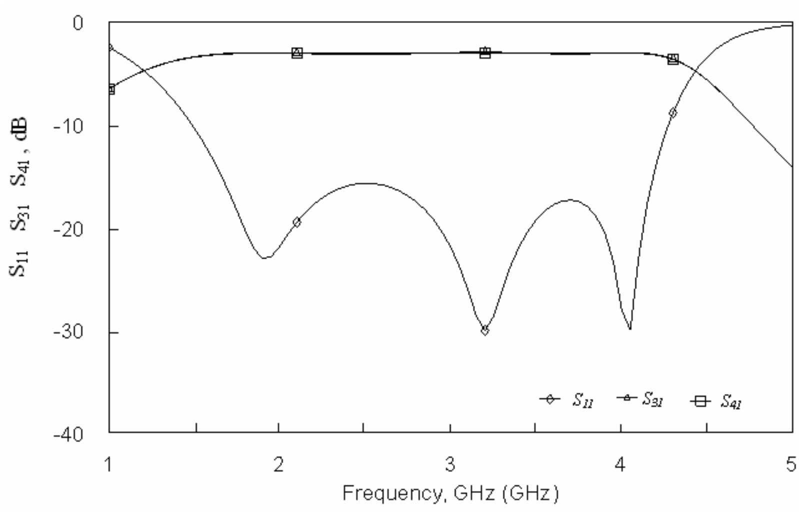

(a)

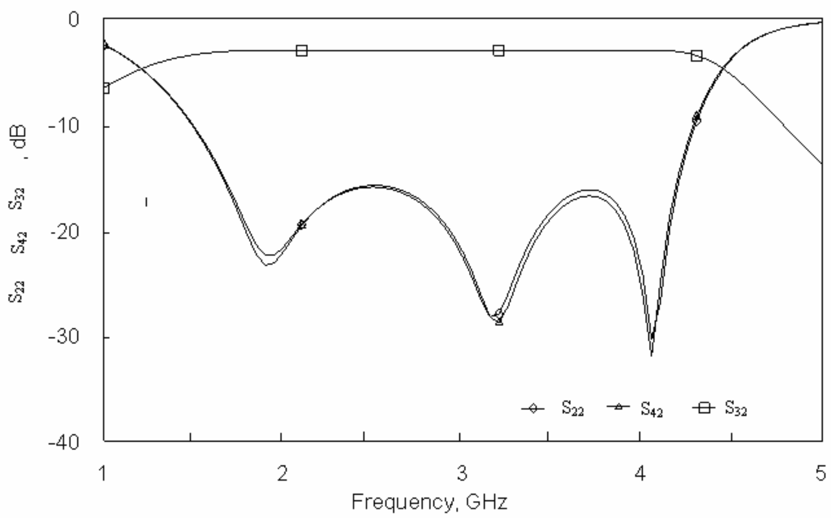

(b)

Figure 4.10: The simulated results of return loss and coupling of the proposed impedance-transforming broadband 180° hybrid ring. (a) Out-of-phase operation. (b) In-phase operation.

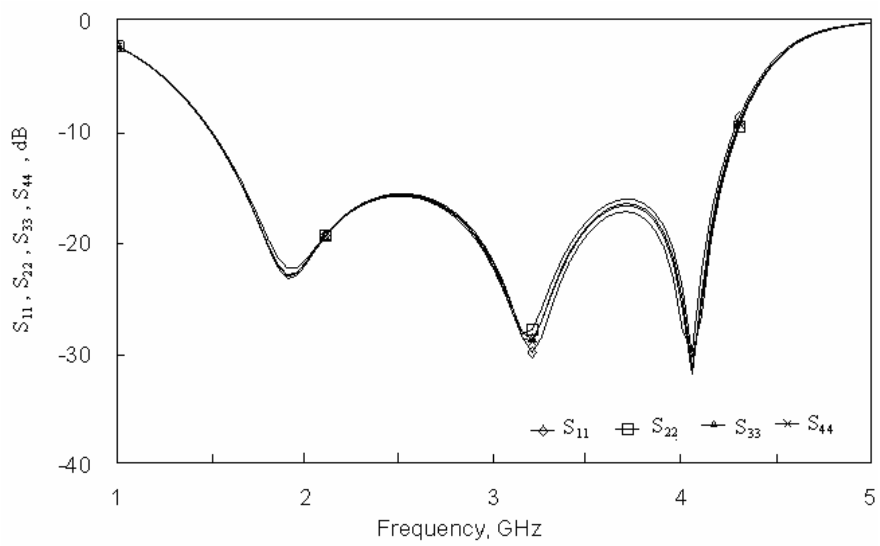

Figure 4.11: Simulated return loss for all the ports of the proposed impedance-transforming broadband 180^o hybrid ring.

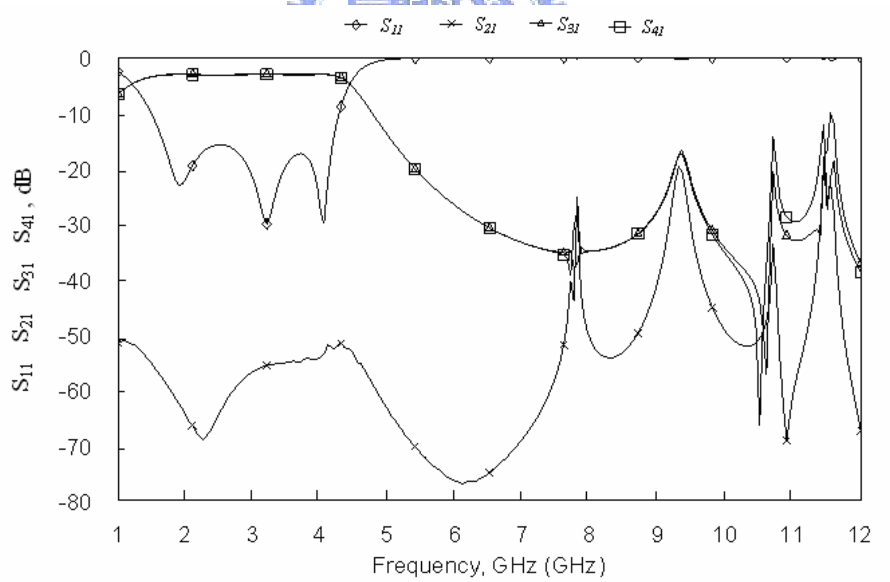

Figure 4.12: Simulated broadband performance of the proposed 180^o hybrid ring.

4.4 Fabrication and Measurements

The circuit is fabricated on Al_2O_3 substrate with 15-mil thickness and a dielectric constant of 9.8. The proposed 180^o hybrid ring is designed to operate at 3 GHz, with equal power division (3dB), bandwidth from 1.5 to 4.5 GHz, and input/output impedance-transforming ratio of 1:3 (40Ω to 120Ω). The passband frequency response of the proposed circuit is shown in Figure 4.13(a) and (b). The measured return loss is better than 10 dB from 1.49 to 4.42 GHz (99%) for out-of-phase operation and from 1.53 to 4.43 GHz (97%) for in-phase operation. The measured isolation is better than 25dB in the passband. The amplitude and phase balance of the coupling parameters (S_{31} / S_{41} or S_{32} / S_{42}) are shown in Figure 4.14(a) and (b). The amplitude and phase balance in the passband are less than 0.55dB and 4^{o}, respectively, for both in-phase and out-of-phase operation.

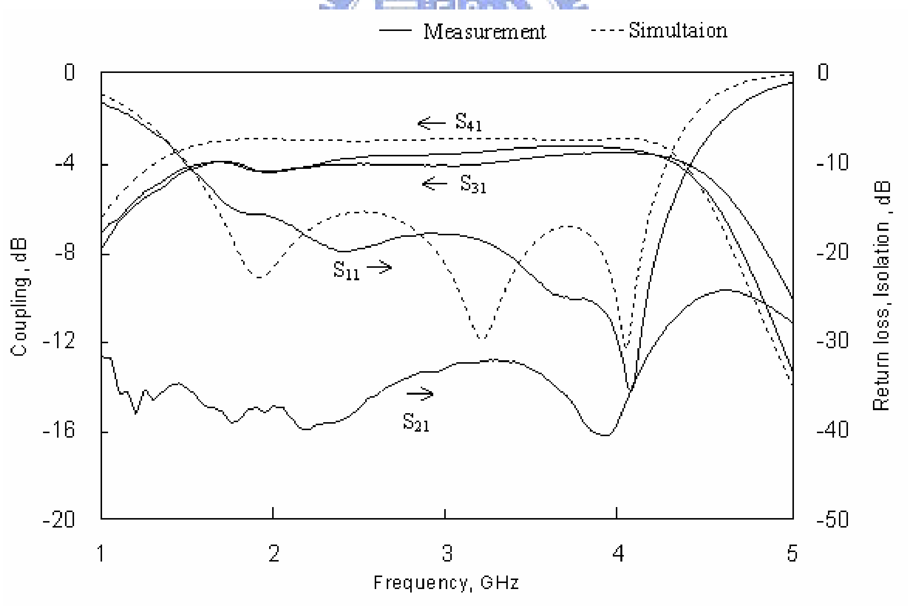

(a)

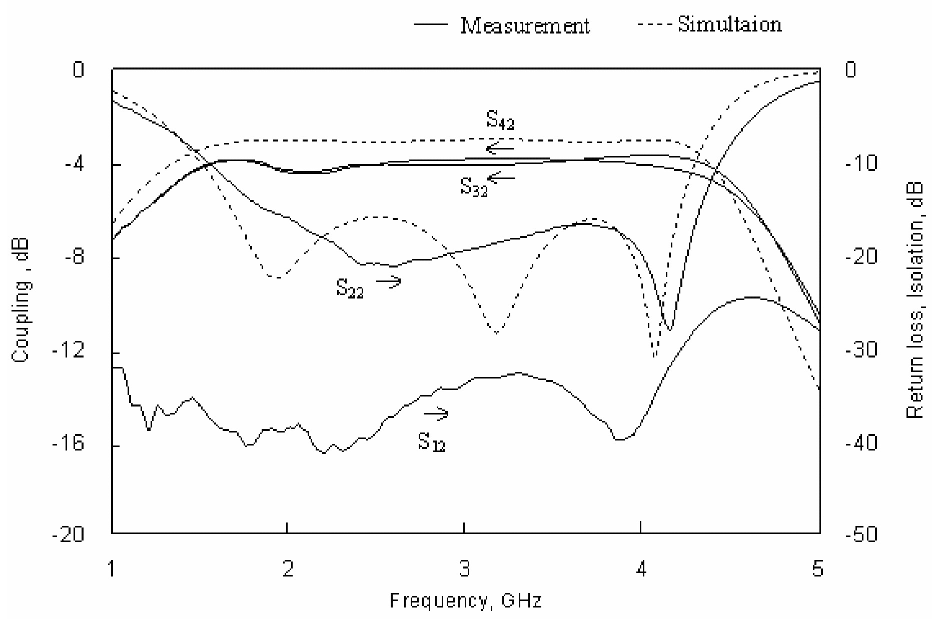

(b)

Figure 4.13: Measured and Simulated results of the proposed impedance-transforming broadband 180^{o} hybrid ring. (a) Out-of-phase operation. (b) In-phase operation.

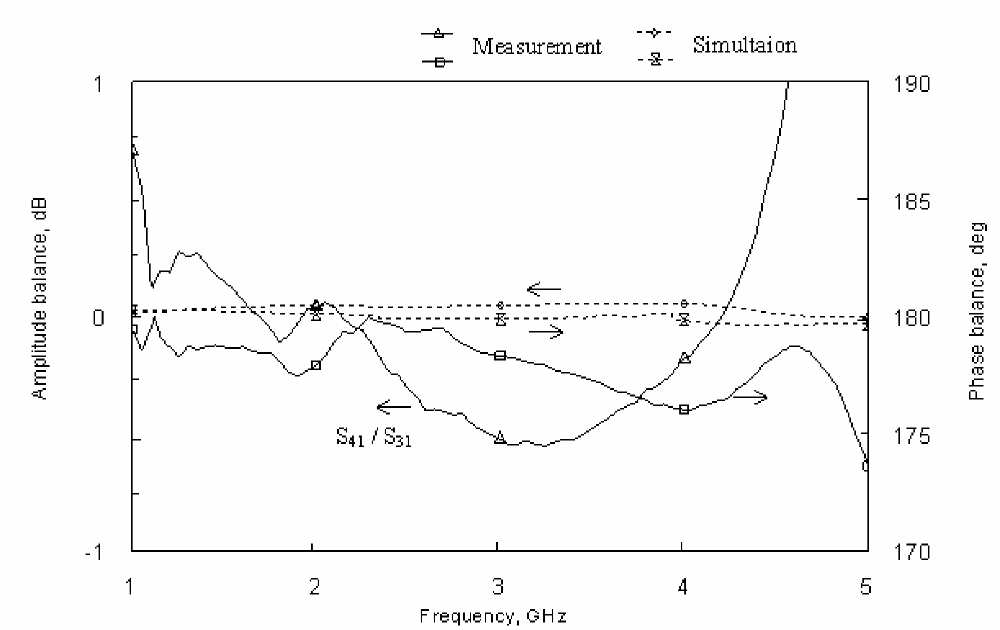

(a)

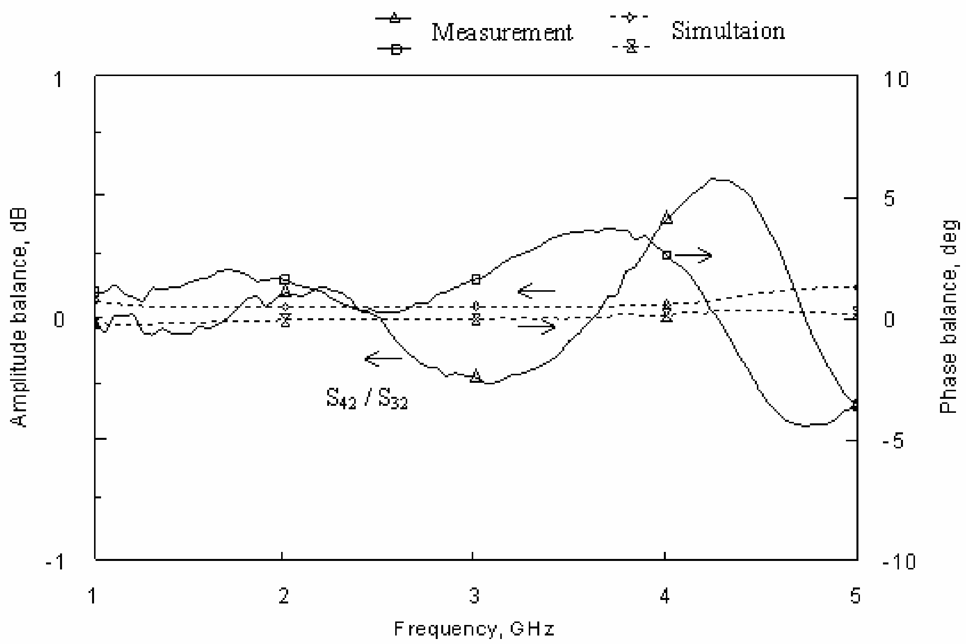

(b)

Figure 4.14: Measured amplitude and phase balance of the proposed impedance-transforming broadband 180^o hybrid ring. (a) Out-of-phase operation. (b) In-phase operation.

Figure 4.15 shows the measured return loss for all the ports of the proposed 180^o hybrid ring. It is shown that the return loss for all the ports in the passband is better than 10dB, so it is verified to be well-matched to the system impedance of 40Ω or 120Ω. The measured broadband performance of the proposed stepped-impedance 180^o hybrid ring is also given in Figure 4.16. It presents no spurious passband up to 10GHz. Figure 4.17 shows the photograph of designed 180^o hybrid ring, of which overall circuit size is 25×25 mm^2.

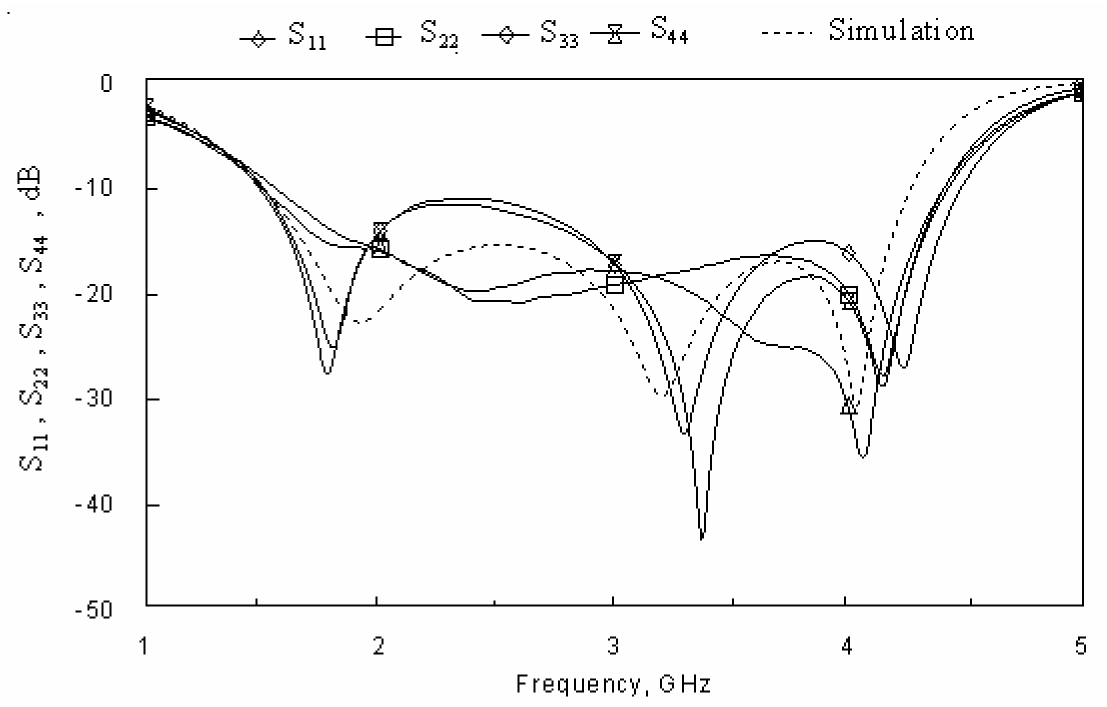

Figure 4.15: Measured and simulated results of return loss for all the ports of the proposed impedance-transforming broadband 180° hybrid ring.

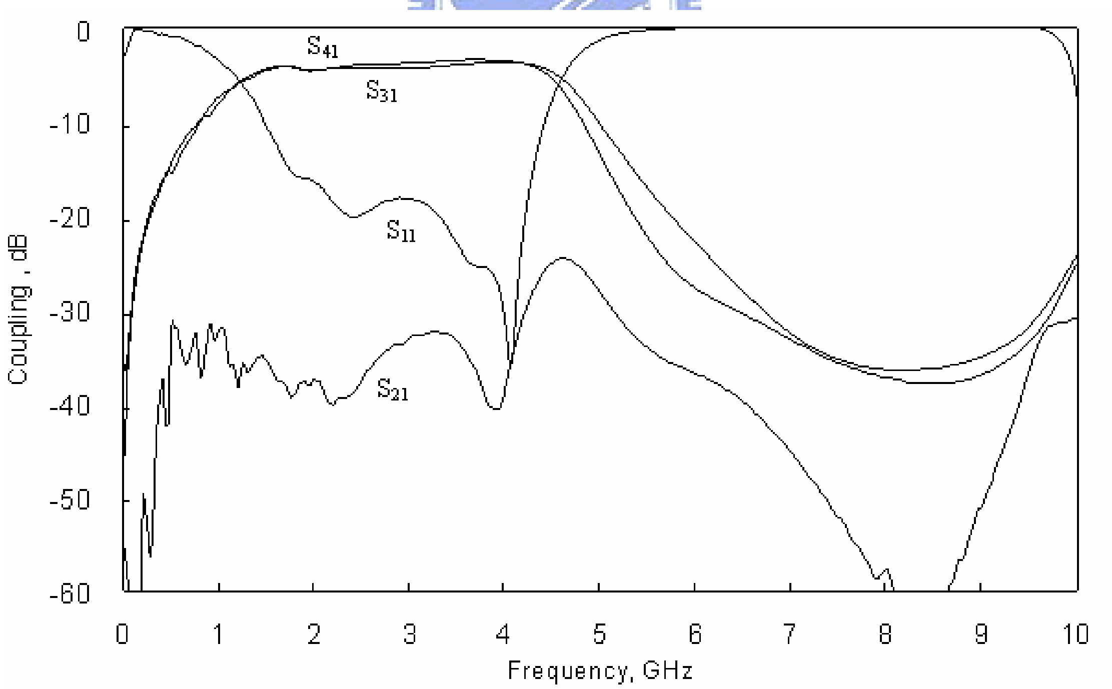

Figure 4.16: Measured broadband performance of the proposed impedance-transforming broadband 180° hybrid ring.

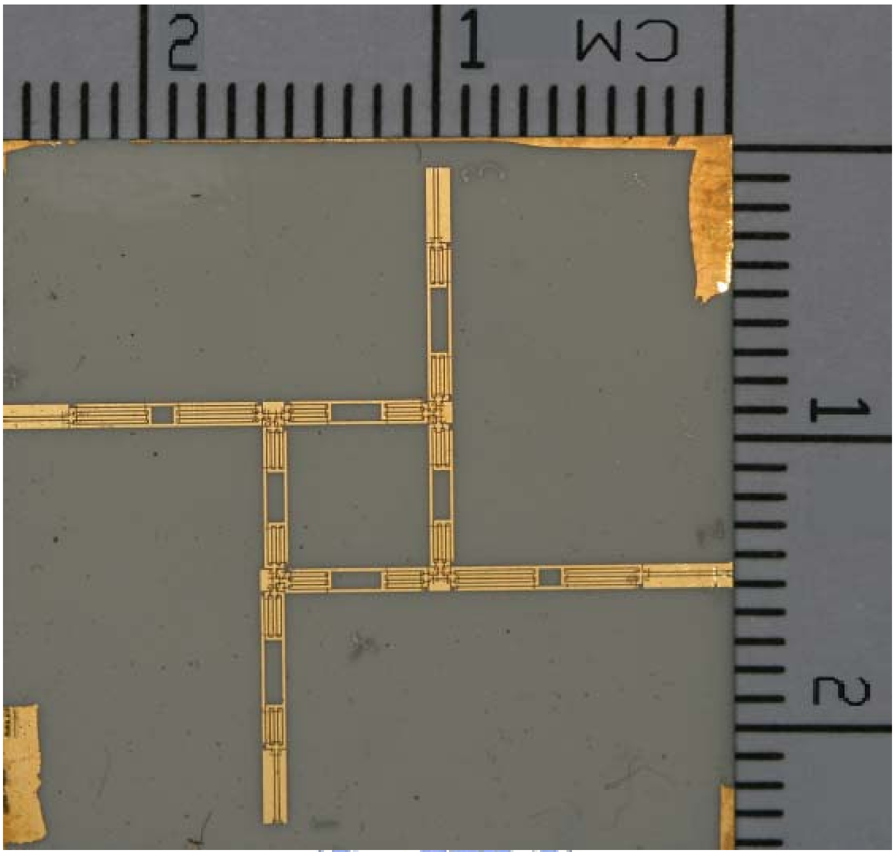

Figure 4.17: Photograph of the proposed impedance-transforming broadband 180° hybrid ring.

Chapter 5
Conclusion

In this study, we proposed two Ku band reflection-type phase shifters, in which four and two varactors are used, respectively. The measured performance covers 12.2-12.7 GHz and can be used for broadcasting satellite service (BSS). In chapter two, a 360^{o} phase shifter with four varactors has been presented. The phase shift of 360^{o} is achieved by the reflection load based on the parallel connection of two series tuned varactors. The reduction of insertion-loss variation is attributed to the impedance transformer between the reflection load and the 3-dB 90^{o} hybrid coupler. Measured results have shown that maximum phase shift is larger than 360^{o}, the insertion loss is 4.8 ± 1.6 dB, and return loss is better than 14 dB over 500 MHz.

In chapter three, a reflection-type phase shifter with two varactors is fabricated and used in a phased array. This work extends the maximum phase shift of the phase shifter from 52^{o} to 286^{o} by resonating the varactor with via inductance and impedance transformers. Theoretically, the insertion-loss variation may be compensated with a resistance parallel to the reflection load. However, the measured insertion-loss variation is improved by only 0.5 dB with the used of compensating resistance due to the parasitic effect of the chip resistor at high frequency. Furthermore, we integrate the phase shifter into a 4-element phased array. The measurement results show that we can change the direction of the main beam by adjusting the control voltage of phase shifters.

In chapter four, the 180^{o} hybrid ring adding a unit element at each port has been designed to exhibit Chebyshev response and impedance transformation. We use hybrid CPS/interdigital CPS as stepped-impedance and ideal phase inverter for size reduction of 70% and wideband performance. The fabricated 180^{o} hybrid ring exhibits a wide bandwidth of almost 100%, and its amplitude and phase balance are less than 0.55dB and 4^{o}, respectively. For system impedance transformation of 40Ω and 120Ω, the four ports of the network are well-matched.

Reference

[1] R. N. Hardin, E. J. Downey, and J. Munushian, “Electronically variable phase shifter utilizing variable capacitance diodes,” *Proc. IRE*, vol. 48, no. 5, pp. 944–945, May 1960.

[2] R. V. Garver, “360 varactor linear phase modulator,” *IEEE Trans. Microw. Theory Tech.*, vol. MTT-17, no. 3, pp. 137–147, Mar. 1969.

[3] J. I. Upsur and B. D. Geller, “Low-loss 360 X-band analog phase shifter,” in *IEEE MTT-S Int. Microw. Symp. Dig.*, Jun. 1990, pp. 487–490

[4] S. Shin, R. V. Snyder, and E. Niver, “360-degree linear analog phase shifter design using tunable short-circuit terminated combline filters,” in *IEEE MTT-S Int. Microw. Symp. Dig.*, May 2001, pp. 303–306.

[5] C. S. Lin, S. F. Chang, and Y. H. Shu, “A full 360 reflection-type phase shifter with constant insertion loss,” *IEEE Microw. Wireless Compon. Lett.* , vol. 18, no. 2, Feb. 2008.

[6] K. O. Sun, H. J. Kim, C. C. Yen, and D. Weide, “A scalable reflection type phase shifter with large phase variation,” *IEEE Microw. Wireless Compon. Lett.*, vol. 15, no. 10, pp. 647–648, Oct. 2005.

[7] B. T. Henoch and P. Tamm, “ A 360 reflection-type diode phase modulator,”

IEEE Trans. Microw. Theory Tech., vol. MTT-19, no. 1, pp. 103–105, Jan. 1971.

[8] Y. H. Liew, J Joe, M.S. Leong , “A novel 360 analog phase shifter with linear voltage phase relationship,” in *Aisa-Pacific Microw. Conf. Dig.*, Singapore, 1999

[9] C. S. Lin, S. F. Chang, C. C. Chang, and Y. H. Shu, “Design of a reflection-type phase shifter with wide relative phase shift and constant insertion loss,” *IEEE Trans. Microw. Theory Tech.*, vol. 55, no. 9, pp. 1862–1868, Sep. 2007.

[10] S. March, “A wideband stripline hybrid ring,” *IEEE Trans. Microw. Theory Tech.*, vol. MTT-16, p. 361, June 1968

[11] B. R. Heimer, L. Fan, and K. Chang, “Uniplanar hybrid couplers using asymmetrical coplanar striplines,” *IEEE Trans. Microw. Theory Tech.,* vol. 45, pp. 2234–2240, Dec. 1997

[12] L. Fan, C.-H. Ho, and K. Chang, “Wide-band reduced-size uniplanar magic-T, hybrid-ring, and de Ronde’s CPW-slot couplers,” *IEEE Trans. Microw. Theory Tech.*, vol. 43, pp. 2749–2758, Dec. 1995.

[13] K.-S. Ang , Y.-C. Leong and C.-H. Lee, “Converting baluns into broad-band impedance-transforming 180^{o} hybrids,” *IEEE Trans. Microw. Theory Tech., vol. 50,* no. 8, pp. 1990-1995, Aug. 2002.

[14] C.-Y. Chang and C.-C. Yang, “A novel broad-band Chebyshev-response rat-race ring coupler,” *IEEE Trans. Microwave Theory Tech.*, vol. 47, pp. 455–462, Apr.

1999.

[15] R. K. Settaluri, G. Sundberg, A.Weisshaar, and V. K. Tripathi, “Compact folded line rat-race hybrid couplers,” *IEEE Microw. Guided Wave Lett.*, vol. 10, no. 2, pp. 61–63, Feb. 2000.

[16] K. W. Eccleston and S. H. M. Ong, “Compact planar microstripline branch-line and rat-race coupler,” *IEEE Trans. Microw. Theory Tech.*, vol. 51, no. 10, pp. 2119–2125, Oct. 2003

[17] Y.-J. Sung, C.-S. Ahn, and Y.-S. Kim, “Size reduction and harmonic suppression of rat-race hybrid coupler using defected ground structure,” *IEEE Microw. Wireless Compon. Lett.*, vol. 14, no. 1, pp. 7–9, Jan. 2004.

[18] T. Hirota, A. Minakawa, and M. Muraguchi, “Reduced-size branch-line and rat-race hybrids for uniplanar MMIC’s,” *IEEE Trans. Microw. Theory Tech.*, vol. 38, pp. 270–275, Mar. 1990.

[19] D.-I. Kim and G.-S. Yang, “Design of new hybrid-ring directional coupler using λ/8 orλ/6 sections,” *IEEE Trans. Microw. Theory Tech.*, vol. 39, no. 10, pp. 1779–1784, Oct. 1991.

[20] C.-H. Chi and C.-Y. Chang, “A wideband CPS bandpass filter with ultra-wide upper stopband using stepped-impedance rat-race hybrid couplers,” in *European Microw. Conf. Dig.*, Munich, Germany, pp. 548-551, Oct. 2007.

[21] J-C Lu and C-Y Chang, "Design and optimization method of an impedance-transformed multisection 180^o hybrid," under preparation to submit to *IEEE Trans. Microw. Theory Tech.*

[22] K. S. Ang, Y. C. Leong, and C. H. Lee, "A new class of multisection 180^o hybrids based on cascadable hybrid-ring couplers," *IEEE Trans. Microw. Theory Tech.*, vol. 50, no. 9, pp. 2147–2152, Sep. 2002.

[23] R. Mongia, I. Bahl, and P. Bhartia, *RF and Microwave Coupled-Line Circuits*, Boston, MA: Artech House, 1999.

[24] K. Kurokawa, "Power waves and the scattering matrix," *IEEE Trans. Microw. Theory Tech.*, vol. MTT-13, no. 3, pp. 194–202, Mar. 1965.